AIAA SciTech Forum
6-10 January 2025, Orlando, FL
AIAA SCITECH 2025 Forum

10.2514/6.2025-1068

On the Application of an Actuator Line Model for Rotorcraft Outwash Predictions

Nicholas Peters * and Dorsa Shirazi †
NASA Ames Research Center, Moffett Field, CA 94035

As the next generation of Vertical Take-Off and Landing (VTOL) vehicles develops and the VTOL industry makes significant progress in utilizing them for public transportation, it is crucial to have validated and cost-effective computational models accessible to both industry professionals and academics in the rotorcraft community. This study investigates the implementation of a new actuator line model within NASA's OVERFLOW computational fluid dynamics (CFD) solver, with a focus on predicting rotorcraft outwash. This reduced-order rotor model was developed to provide reasonably accurate outwash predictions while reducing computational costs compared to traditional blade-resolved CFD simulations. To validate the actuator line model for outwash predictions, the model was compared against existing experimental data across three validation cases: single rotor Out-of-Ground Effect (OGE), single rotor In-Ground Effect (IGE), and tandem rotor IGE. All three cases were based on the rotor geometry and configuration of the CH-47D. To evaluate the feasibility and advantages of using an actuator line model for outwash predictions the results were compared to a series of high-fidelity blade-resolved CFD simulations as well as comprehensive analyses simulations based on CHARM predictions. The results of this study demonstrate the feasibility of leveraging this new actuator line model for reasonably accurate outwash predictions. The outwash results obtained from the actuator line model closely matched those from high-fidelity blade-resolved simulations while significantly reducing the overall computational costs of the simulations. Results from this study further demonstrated the feasibility of using CHARM for efficient, and reasonably accurate time-averaged outwash predictions for multi-rotor configurations.

I. Nomenclature

h	=	rotor height above ground, ft
p	=	pressure, psi
q	=	the heat flux vector, Btu/h.ft^2
r	=	radial distance from the aircraft reference center, ft
t	=	time, s
u	=	velocity vector, ft/s
z	=	coordinate normal to the ground, ft
E	=	energy, J
F	=	the source term vector
Pr	=	Prandtl number
R	=	rotor radius, ft
Re	=	Reynolds number
a_1	=	diffusion gain constant
c_d	=	section drag coefficient
c_l	=	section lift coefficient
c_m	=	section moment coefficient
r_{c_0}	=	initial element core size, ft
v_h	=	hover induced velocity using momentum theory, ft/s

*Aerospace Engineer, Aeromechanics Office, Mail Stop 243-12.
†Aerospace Engineer, Aeromechanics Office, Mail Stop 243-12.

x_o, y_o, z_o	=	three-dimensional position of the current J-node
A_{PAXman}	=	frontal area of a ground personnel as modeled using the PAXman model, ft
C_D	=	drag coefficient
C_L	=	lift coefficient
C_M	=	moment coefficient
C_T	=	thrust coefficient
F_{PAXman}	=	forces on ground personnel
V_r	=	outwash velocity, ft/s
V_{tip}	=	rotor tip velocity, ft/s
V_z	=	component of velocity along the z-coordinate, ft/s
α	=	angle of attack, deg
ϵ	=	smoothing factor
ρ	=	density, lb/ft^3
τ	=	shear stress, lb/ ft^2
ν	=	kinematic viscosity, ft^2/s
Γ_v	=	vortex circulation strength, ft^2 /s
AAM	=	Advanced Air Mobility
$ACERO$	=	Advanced Capabilities for Emergency Response Operations
AMR	=	adaptive mesh refinement
$APEX$	=	U.S. Army Advanced Prototyping Engineering and Experimentation
$BCVE$	=	Basic Curved Vortex Elements
CFD	=	computational fluid dynamics
CGT	=	chimera grid tool
CVC	=	constant vorticity contour
DES	=	detached eddy simulation
HFV	=	hierarchical fast vortex method
IGE	=	in ground effect
MPI	=	message passing interface
$N-S$	=	Navier-Stokes
OGE	=	out of ground effect
PIV	=	particle image velocimetry
$RVLT$	=	Revolutionary Vertical Lift Technology
UAM	=	Urban Air Mobility
$URANS$	=	unsteady Reynolds averaged Navier-Stokes
$VTOL$	=	vertical take off and landing
$VVPM$	=	viscous vortex particle method

II. Introduction

The topic of outwash/downwash predictions has long been of high interest to the rotorcraft community. Due to the high velocities typically induced by Vertical Take-Off and Landing (VTOL) aircraft, as early as the 1960s, researchers had identified the significant danger outwash/downwash imposes on vehicle operators and ground personnel [1]. Early studies indicated that for relatively low levels of outwash ($\leq$ 15 knots), there is still an acute need for protective wear to guard both the eyes and exposed skin against small particulates near the landing pad [2]. In cases where the generated outwash exceeds 48 knots (velocities not uncommon for rotorcraft ground operations) ground personnel and equipment are exposed to a notably higher degree of danger as nearby objects (tree limbs, roofing, and bricks) may become detached, leading to the injury of those near the landing pad [3]. In addition to posing risks for the ground crew, outwash additionally exposes the vehicle and airborne crew to heightened levels of danger as well. Generated outwash profiles often limit the proximity within which rotorcraft can operate. An additional notorious example includes the brownout/whiteout problem, which occurs when rotorcraft hover over dry, loosely compacted sand/snow. Under such conditions, dust particles can get entrained in the rotor's downwash, leading to a significant reduction in pilot visibility and dust being ingested into the rotorcraft's propulsion system. In the early 2000s, the U.S. Army spent approximately $100 million per year on maintenance costs related to brownout. Further, brownout was reportedly responsible for three out of every four rotorcraft accidents in Iraq and Afghanistan [4].

Given the substantial levels of risk associated with the outwash problem, a collaboration of government, university, and private institutions has contributed significant resources towards understanding the problem. These contributions have resulted in extensive literature covering mid- and high-fidelity numerical studies [5–7] and experimental surveys [8, 9]. While further work in the field is warranted, current progress made on the outwash topic by the rotorcraft community has resulted in a detailed knowledge of experimentally determined outwash profiles and various numerical approaches for predicting said profiles. However, despite the significant resources applied, historical experience with the outwash problem has predominately focused on single main rotor, tandem rotor, and tiltrotor configurations. These rotor configurations are not consistent with typical proposed VTOL Advanced Air Mobility (AAM) designs. As the aviation community continues to mature the field of VTOL AAM, historical experience with the outwash problem suggests a new effort for both accumulating experimental measurements and validating numerical approaches is warranted.

Typical AAM missions are defined by having a range below 500 nm, encompassing rural and urban operations, and used for passenger and cargo-based payloads. Previous efforts in the AAM field have focused on both improving regional and urban air mobility. However, recent efforts of both NASA's Revolutionary Vertical Lift Technology (RVLT) [10–12] and Advanced Capabilities for Emergency Response Operations (ACERO) [13] projects have begun investigating the broader application of AAM for public good missions [14]. Given the broad range of potential mission profiles VTOL AAM may operate within, it becomes imperative that high-fidelity outwash predictions can feasibly be obtained. However, the scope of potential rotor configurations to analyze for VTOL AAM remains a significant challenge in obtaining these predictions, particularly within the context of vehicle conceptual design. For an appreciation of the vast scope of potential rotor configurations an AAM vehicle may have, readers are encouraged to review the eight NASA Urban Air Mobility (UAM) reference models [15]. Said reference models range from a two-rotor (Side-by-Side) to a six-rotor (Multi-Tiltrotor) to an eight-rotor (Lift+Cruise) rotor configuration, with a four-rotor quadrotor configuration also included. Previous experience in the field has demonstrated rotor outwash generated by a single-rotor vehicle is notably different from even a tandem or tiltrotor vehicle. As early as the 1980s, studies focused on the influence of rotor configuration on outwash highlighted that for tiltrotor VTOL aircraft, the generated outwash becomes highly directional [16]. When compared to a single-rotor design, tiltrotor vehicles tend to produce outwash profiles that contain regions of high-velocity outwash, with velocities much higher than would be produced by a comparable single-rotor design. These regions of high-velocity outwash tend to occur at the intersection of the two rotors' wakes. These regions of high-velocity outwash are located on the forward and aft regions of the XV-15 [16] and the port and starboard side of a CH-47 [9]. For VTOL AAM style aircraft, proposed rotor configurations are often more complex than those of historical tandem and tiltrotor designs, leading to a need for increased rigor in feasibly achieving accurate numerical prediction of VTOL AAM outwash profiles [17]. The challenges are further exacerbated by the insufficient availability of experimental measurements that accurately represent VTOL AAM vehicles.

Given the lack of experimental measurements and the aerodynamic complexities associated with the outwash problem, a variety of mid-fidelity low computational cost numerical approaches have been proposed and investigated in recent years. For example, to address the critical issue of "brownout" for U.S. Army rotorcraft, the U.S. Army and Continuum Dynamics, Inc. (CDI) worked together to develop a physics-based brownout model [5] to capture the complex flow field generated by rotorcraft near the ground. CDI's CHARM code was used to validate the wake model for a single rotor in the presence of the ground without including the fuselage against the experimental data of CH-53 and XV-15 rotorcraft flight test data [18]. The CHARM predictions for peak and average rotor outwash well matched the experimental results.

Recent studies [19–21] have established meaningful computational approaches that may become the cornerstones of future VTOL AAM outwash investigations. However, in the absence of wider accessibility to VTOL AAM-specific experimental measurements, thorough validation of said numerical approaches remains challenging. Without robust experimental validation data, designers are pushed to rely on the highest fidelity modeling approaches feasibly available. In a recent study completed out of NASA Ames, a series of high-fidelity Detached Eddy Simulation (DES) based Computational Fluid Dynamics (CFD) simulations were completed for both a single and quad-rotor configuration [22]. The results of the single rotor showed a close comparison with experimental measurements while quadrotor predictions indicated regions of high velocity outwash across the vehicle's longitudinal and lateral axes. Furthermore, the magnitude of simulated outwash velocities was defined as *hazardous* by the study, thus reinforcing the need for studies such as the present one.

Yet, full-order blade-resolved CFD simulations remain prohibitively expensive for large-scale parametric studies of rotor configurations. A significant contributing factor to this increased computational cost is the expense required to accurately implement a blade-resolved model within a CFD simulation. Owing to the aerodynamically complex, three-dimensional, time-dependant, rotational flow, accurate blade thrust and power predictions often require high levels

of mesh refinement, typically requiring a y^+ near 0.1 for the first cell of the wall [23]. Furthermore, complexities of the surface flow field require small time step sizes, often recommended at an azimuthal 0.25-degree blade rotation per time step. Conversely, previous experience in the field has demonstrated outwash is often largely determined based on a combination of rotor thrust coefficients rather than rotor blade geometry. As such, one practical approach for reducing computational cost while largely retaining simulation fidelity is potentially available through the implementation of an actuator line modeling approach. In this approach, the blade mesh is replaced with a blade element lifting line model. Blade spanwise loads are either computed or prescribed and introduced into the CFD solver through the use of energy and momentum source terms. The goal of implementing the actuator line model is to reduce the computational cost associated with the blade body mesh while retaining the CFD fidelity of the off-body solver.

Currently, there is no actuator line model available in NASA's OVERFLOW CFD solver, which is commonly used in the RVLT project [24–26] and by the wider rotorcraft community [27, 28]. Therefore, this study implements a preliminary actuator line model in the OVERFLOW CFD code to analyze downwash and outwash predictions for both single and tandem hovering rotors. In implementing this model, the study aims to achieve two main objectives. The first objective of this study is to evaluate the relative fidelity and computational cost of actuator line and blade-resolved time averaged outwash predictions. The second objective is to explore the potential role of the actuator line model within contemporary rotorcraft design toolchains. As highlighted earlier, the actuator line modeling approach aims to provide a level of modeling fidelity similar to that of blade-resolved CFD simulations, while significantly reducing computational costs. However, compared to mid-fidelity panel method solvers the actuator line modeling approach will require substantially more computational resources. To quantify the actuator line predictions in terms of modeling fidelity and computational cost, this study further includes both blade-resolved CFD simulations and CHARM-based vortex lattice method simulations. Predictions will be presented for three demonstration cases. The first case will showcase actuator line predictions for a single rotor hovering out of ground effect (OGE). The results for the OGE case will focus on rotor wake structures, blade loading, and induced velocity profiles at various distances below the rotor's hub. The second case will present actuator line predictions for a single hovering rotor in ground effect (IGE), evaluating blade loading, the maximum outwash velocity as a function of radial distance from the rotor's hub, and the rotor outwash profile at varying distances from the hub. The third case will replicate the second case but with a tandem rotor configuration instead. For both outwash prediction cases, time averaged outwash predictions are further integrated through use of the PAXman model [3]. Simulation results for all three cases will be compared to experimental measurements [8, 9].

This paper is organized as follows. First, implementation of the actuator line model as used in this study is presented in the section *Actuator Line Methodology*. Next, the case setup for all numerical simulations are reviewed in section *Numerical Approach*. Finally, all results are presented and discussed in section *Results and Discussion*, while all concluding remarks are found in *Conclusions*.

III. Actuator Line Methodology

In this section, an overview of the implemented actuator line modeling approach will be presented. The implemented grid generation approach will first be presented, outlining both the selected meshing approach along with identified best practices. Next, a summary of the mathematical approach selected for the lifting line model will be provided.

A. Grid Generation Approach

The actuator line model used in this study was implemented on a single block rectangular structured grid. As will be discussed in the *Numerical Approach* section, this single block near-body grid is then overset with a series of Cartesian multi-block off-body grids. To generate the actuator line grid, NASA's grid generation software Chimera Grid Tool (CGT) was used. The actuator line mesh is defined using three orthogonal node directions, labeled in this paper as J, K, and L nodes. Grid J-nodes are more distributed along the rotor's spanwise direction. To help resolve rotor tip vortex formation, J-nodes are concentrated at the rotor's tip and root with a spanwise spacing of 2% of the corresponding mean chord length. Grid J-nodes are then extruded 20% of the rotor's radius from the rotor's tip and root with a growth rate of 1.2. As noted by previous works, when implementing overset gridding approaches in a CFD solver care must be taken to ensure coherent features of the flow field are well formed before being passed between overset grids [29]. Given this study is a preliminary work on the implementation of an actuator line modeling within the OVERFLOW solver, an overly conservative extrusion distance of 20% a rotor's radius was selected. Further work is needed to identify a less conservative, and more computationally efficient, extrusion distance. Grid K-nodes are then, in a similar manner, extruded from the actuator line nodes in the chordwise direction, while the L-nodes are

extruded in the thrust direction. While further work is warranted, preliminary grid independence studies completed in this study suggest a grid-independent solution can be achieved with 100 spanwise J-nodes used between the root and tip, and 50 J, K, and L-nodes used to extrude off the actuator lines surface with a growth rate of 1.2. As described in the following subsection, source terms for each blade are then distributed along the J-nodes between the rotor's root and tip. To represent a given rotor, a single block grid represents a single blade of the rotor system. As such, to implement a multiple-bladed rotor, this blade grid must be duplicated and distributed about the axis of rotation. Hole cutting is specified such that no blade mesh overlapping occurs in the rotor root cutout.

B. Implemented Source Term Model

With each rotor's respective grids placed about the axis of rotation, a series of inputs are required on the part of the user such that blade sectional loads can be computed. In this preliminary implementation of the actuator line model, geometric inputs are limited to linear twist and taper distributions, rotor radius, collective, and a source term smoothing parameter which will be discussed at the end of this subsection. At each time step, the local loading coefficients must be computed for each J-node along the spanwise direction of the rotor. An essential step in computing the load coefficients is the extraction of induced velocities at each blade element location. The extraction of said induced velocities continues to be a significant area of research in the sub-topic of actuator line modeling [30]. A quick review of the literature will show a plethora of available approaches for extracting induced velocities and the identification of the proper approach for rotorcraft applications warrants further investigation [31, 32]. However, said investigation remains outside the scope of this study, and as such a single induced velocity extraction approach was implemented. In this approach, a Guassian kernal is used to average induced velocities in the near vicinity of the given blade element. As outlined by both Forsythe [33] and Churchfield [34], it can be demonstrated, at least for a 2D airfoil, that the free stream velocity of a given blade element is equal to the integration of the velocity field over the Gaussian kernal, assuming this same kernal function is applied to the source term as well. In this study, the below kernal is used.

$$\Phi(x, y, z) = \frac{1}{\epsilon^3 \pi^{3/2}} \exp - \frac{(x - x_o)^2 + (y - y_o)^2 + (z - z_o)^2}{\epsilon^2} \tag{1}$$

$$\int_{-\infty}^{\infty} \int_{-\infty}^{\infty} \int_{-\infty}^{\infty} \Phi(x, y, z) dx dy dz = 1 \tag{2}$$

In Eqn. 1, Φ is the Gaussian distribution function, ϵ a smoothing factor, (x, y, z) are three-dimensional spatial positions to be distributed over, and x_o, y_o, and z_o is the three-dimensional position of the current J-node. The Gaussian distribution function is defined such that the three-dimensional integral, shown in Eqn. 2, is equal to 1. The smoothing factor ϵ is then used to determine the volume over which the kernal will be applied.

In the original approach, this kernal was applied as a spheroid to average across a volume of near-nodes to the blade element. However, in this study an alternative approach is implemented. In this approach, the kernal is applied only to the L/K plane bounding the given blade element. By specifying no MPI cutting in the L/K plane, this alteration allows the extraction to take place within a single MPI rank, reducing computational cost and rigor in searching and communicating between MPI ranks. This new kernal is normalized such that Eqn. 2 holds within the given MPI rank.

After extracting the induced velocities, local angles of attack are then computed based on the extracted induced velocity, angular rotation of the rotor, radial location and twist of the blade element, and the applied collective. The local angle of attack, along with the freestream velocity as computed at the given radial station, is then used to reference an airfoil performance look-up table such that sectional loads can be efficiently computed. Typically, said look-up tables are either generated through extensive experimental measurements [35] or through carefully conducted CFD-based surveys [36] or a combination of both options. In implementing any actuator line-based modeling approach for rotor performance predictions, a well validated, comprehensive airfoil performance table must be available and capable of providing airfoil lift, drag, and moment predictions across a variety of angles of attack and Mach numbers [37]. After extracting local load coefficients, these coefficients are then dimensionalized based on local area, density, and velocity. A simplified tip loss model is implemented by tapering sectional loads beyond the 98% radial station to zero with a linear taper function (function output at a radial station of 98% is 1 and the output at the tip is 0). In this preliminary study, only lift coefficients are included as source terms in the energy and momentum equations.

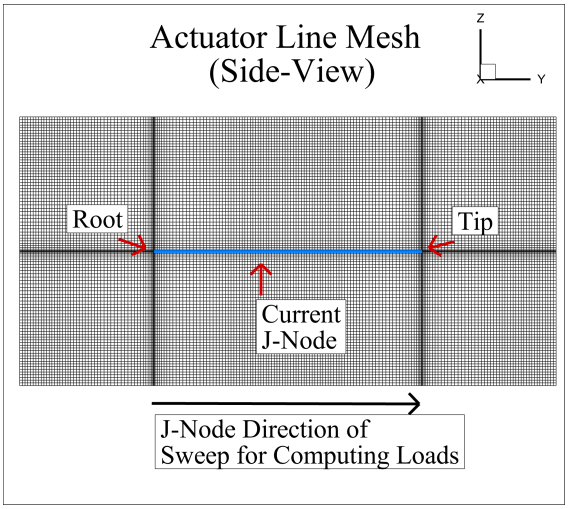

Fig. 1 Z-Y Plane view of actuator line mesh. Graphic shows root and tip J-nodes along with sweep direction used for computing rotor loads.

As a final step before adding the source terms to the energy and momentum equations, a source distribution function was applied to distribute each source term over multiple cells. This source distribution function was implemented with the aim of improving the numerical stability of the derived model. While multiple source distribution functions exist in the literature, the three-dimensional Gaussian distribution function was selected for this implementation and is shown in Eqn. 1. As outlined in the NASA LAVA implementation of the actuator line model, selection of ϵ will depend on blade geometry and grid resolution [38]. In this study, ϵ was fixed and equal to the mean chord length. The same ϵ value was used for both inflow extraction and source term distribution.

IV. Numerical Approach

With the actuator line methodology outlined, this section summarizes each numerical simulation. This study focuses efforts on evaluating the derived actuator line model around three demonstration cases; single rotor OGE, single rotor IGE, and tandem rotor IGE as outlined in Fig. 2. All three cases were selected such that a validation study could be completed comparing numerical approaches against experimental measurements reported both by Ramasamy and Yamauchi [9], and Silva and Riser [8]. In the first case, measurements are reported for a single rotor OGE, Fig. 2 (a). The scaled rotor system used a 1/57th scaled CH-47D rotor with a rotor radius of 0.526 ft, three blades, a solidity of 0.057, and a tip speed of 194.9 ft/s. The blade airfoil was a custom-made low Reynolds number airfoil. For each case, rotors were trimmed to a targeted thrust coefficient of 0.0061. This experimental study was completed in the U.S. Army hover chamber (25 ft x 25 ft x 30 ft) at NASA Ames Research Center. The selected facility was chosen such that a relatively large testing section could be used thus minimizing recirculation effects. During each run, a Particle Image Velocimetry (PIV) imaging recorded 500 image pairs at a sampling rate of 0.49 Hz. For the single rotor OGE case, PIV measurements for induced velocity were recorded at a distance up to 3 rotor diameters beneath the rotor's hub. Measurements were averaged and reported at 9 distinct distances beneath the rotor's hub. This initial validation case is used to gather fundamental insight into the ability of the actuator line model to predict hovering rotor wakes. The second case investigated in this study was that of the single rotor IGE, Fig. 2 (b). In this case, the rotor is fixed at a height of 0.578 rotor diameters from a ground plane. Results published by Ramasamy and Yamauchi demonstrated that outwash characteristics of a single rotor match well with the outwash in the forward region of a CH-47D. As such, in this study, single rotor outwash predictions are compared against full scale outwash measurements in the forward region of a CH-47D as reported by Silva and Riser. In Silva and Riser's experiment, a full-scale CH-47D was hovering at a rotor height of 0.578 diameters and with a thrust coefficient of 0.0061. Measurements were then taken at azimuth locations of $0°, 90°, 180°$, and $270°$ and radial locations ranging from 24 to 180 feet. For the single rotor IGE case, Fig. 2 (b), measurements reported at an azimuth of $0°$ was used. In the final case, Fig. 2 (c), measurements reported for azimuths of $90°$ (starboard) and $270°$ (port) were used. Figure 3 provides a top down graphic of the tandem rotor configuration. In Figure 3, radial axis in the starboard direction is shown in red, radial axis for port direction is shown as dashed green, forward rotor is shown with counter clockwise (CCW) rotation, and aft rotor is shown with clockwise (CW) rotation.

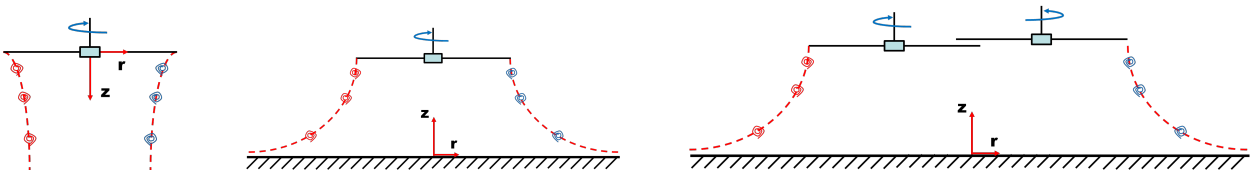

(a) OGE (b) Single Rotor IGE (c) Tandem Rotor IGE

Fig. 2 Side view of configurations simulated in this study.

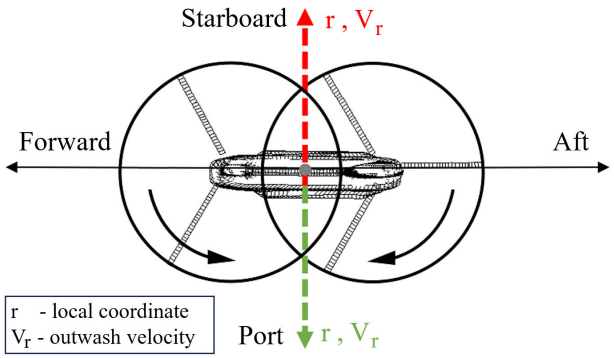

Fig. 3 Top down view of tandem rotor configuration. Radial axis in starboard direction is shown in red and radial axis for port direction is shown as dashed green.

In addition to comparing rotor outwash velocity profiles, outwash predictions using each numerical approach are compared using the PAXman model. The PAXman model is a anthropometric model used to compute forces on representative ground personnel. To use the PAXman model, outwash boundary layer is integrated up to a height of 5.5 feet using Eqn. 3 and represent the force on a 6-ft PAXman crouched and leaning while immersed in outwash. In Equation 3, F_{PAXman} is the predicted force on ground personnel, u is the outwash velocity, and dA_{pax} is the incremental frontal area of the ground personnel crouched and leaning in the outwash.

$$F_{PAXman} = \int \frac{1}{2}\rho u^2 dA_{pax} \tag{3}$$

For each of the three cases, two CFD-based simulations are presented, both using NASA's OVERFLOW CFD solver. The OVERFLOW code is a CFD solver developed by NASA and uses a series of structured, overset grids to numerically model fluid flows. The solver employs a series of high-order discretization approaches, is capable of modeling compressible and transonic flows, performing adaptive mesh refinement, and allowing for both Unsteady Reynolds Averaged N-S (URANS) and turbulence resolving approaches. As such, the OVERFLOW CFD solver has seen extensive use throughout the rotorcraft community. In this study, the OVERFLOW CFD code was utilized to complete both blade-resolved and actuator line-based CFD simulations. In both cases, a 3rd-order central differencing scheme was used for the near-body grids while a higher-order 5th order accurate scheme was used for the off-body solution. Both the blade-resolved and actuator line models used a dual solver approach whereas near-body solutions used the single equation Spalart-Allmaras turbulence model with curvature corrections while the off-body solution was solved using a laminar flow model. The CFD cases were modeled using a full-scale CH-47 rotor with a tip Mach number of 0.61. In experiment completed by Ramasamy and Yamauchi [9], a 6.31 inch rotor was used for a 1/56 sub-scale CH-47 model. As such, in this study a 29.45 ft rotor radius is used for all numerical approaches. Unlike CHARM, in both CFD simulations an integrated trimming model for matching experimental thrust coefficients was not used. As such, while all CFD simulations were targeted for a thrust coefficient of 0.0061, final thrust coefficient was different for each CFD case. For the blade-resolved cases, thrust coefficient was 0.0048, 0.0050, 0.0048 for cases (a), (b), and (c) respectively as labeled in Fig. 2. For the actuator line cases, thrust coefficient was 0.0056, 0.0061, 0.0053 for cases (a), (b), and (c) respectively. To account for this change in thrust coefficient, all results presented in this study are normalized by thrust coefficient. Outwash and downwash results are normalized by momentum theory computed induced velocity,

blade sectional loads are normalized by thrust coefficient. To obtain PAXman model predictions, outwash profiles are re-dimensionalized assuming a thrust coefficient of 0.0061 for each case. While achieving a consistent thrust coefficient between all simulations would be ideal, previous outwash studies completed by Wadcock have demonstrated for radial distances greater than $\frac{r}{D} \geq 1.5$ outwash of a rotor at a given height is self-similar once normalized by thrust coefficient and/or tip mach number scaling [39]. Wadcock findings held for variations in thrust coefficient as high as 100%. These findings are substantiated by full-scale sub-scale outwash scaling as compared by Ramasamy and Yamauchi [9]. As such, the current normalization implemented in this initial study was deemed permissible.

For the single rotor OGE case, solutions were run for 20 rotor revolutions before extracting induced velocity profiles. For both the single and tandem rotor IGE cases, 30 rotor revolutions were completed to generate an initial outwash profile. Outwash profiles were then saved every 10 degrees of azimuth rotor rotation and averaged over the course of 10 rotor revolutions. For the blade-resolved cases, following recommendations commonly found in the literature, a time step corresponding to 0.25-degree rotation of the rotor was selected. For the actuator line cases, a preliminary time step sensitivity study indicated that a time step corresponding to 2-degree rotation of the rotor was sufficient for rotor wake predictions.

To generate the blade-resolved rotor mesh, the RotorGen code was used [40]. The RotorGen code is a recently developed Python-based framework that uses NASA's CGT to automatically generate both rotor volume meshes and all supporting files required to simulate hovering and forward flight rotors in OVERFLOW, all using simplified blade planform definitions and operating condition definitions. The objective of the RotorGen code is to rapidly generate high-fidelity CFD simulation cases from inputs utilized in common rotorcraft-based comprehensive analysis tools. In this study RotorGen was used to generate an OVERFLOW simulation case for a hovering rotor with a linear twist of -20 degrees, no taper, and a NACA-0012 airfoil cross-section. Each blade's surface mesh is split between 7 overset surface grids. For the blade planform mesh, a total of 275 chordwise nodes, 128 spanwise nodes, and 100 normally extruded nodes were used. The root and tip grids are then split between three overlapping subgrids: a leading edge, a center line, and a trailing edge grid. A visualization of the grid system used for the blade tip is provided in Fig. 4. Each surface grid was generated using roughly 10,000 nodes and was additionally normally extruded using 100 nodes. All blade surface grids were extruded half the mean chord length from the blade surface.

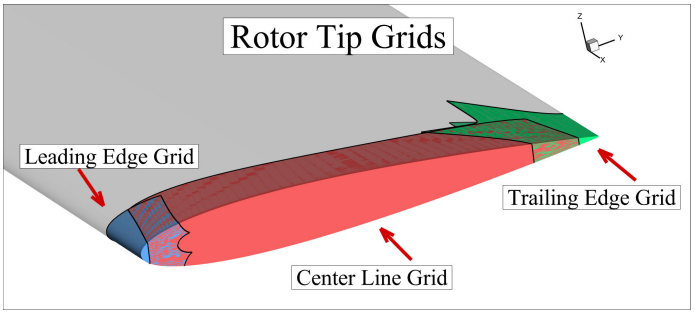

Fig. 4 Visualization three overset surface grids used to mesh blade tip.

For the single rotor OGE case, an initial off-body mesh was generated using two prescribed refinement levels near the blade. A single Cartesian mesh was defined using a uniform spacing of 20% mean chord length and extended 65% radius beneath the hub, 35% radius above the hub, and 20% radius from the rotor's tip. A second, coarser Cartesian mesh was defined using a uniform spacing of 40% mean chord length and extended a further 2 radii beneath the hub. As the case was running, a two-level automatic mesh refinement (AMR) approach was used with the most refined level corresponding to a refinement of 5% mean chord length. A visualization of the blade-resolved off-body mesh after 20 revolutions is shown in Fig. 5. Figure 5 shows the four refinement levels used in this study superimposed on a X-plane extract for vorticity magnitude. In Fig. 5, ΔS corresponds to a spacing of 40% mean chord length. The same off-body grid generation approach was used for both the blade-resolved and actuator line simulations.

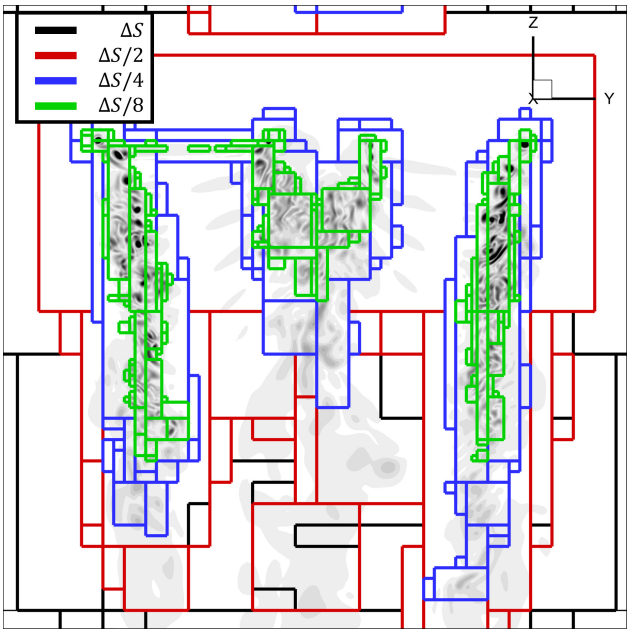

Fig. 5 Visualization of off-body mesh refinement regions after 20 revolutions for the blade-resolved CFD simulation. Four levels of refinement are superimposed on X-plane contours for vorticity magnitude.

CHARM is a comprehensive VTOL aircraft analysis developed by Continuum Dynamics, Inc. (CDI). CHARM uses a combination of fast vortex and fast panel methods to efficiently and accurately model the aircraft's aerodynamic and dynamic interactions and provide information on performance, loads, trim, wake geometry, and surface pressure [41–45].The calculations performed in this paper used CHARM's efficient Constant Vorticity Contour (CVC) wake model [41, 42].The CVC model uses multiple, equal-strength, vortex filaments comprised of Basic Curved Vortex Elements (BCVE's) [43] that lie along contours of constant vorticity to model the trailing vortex sheets along the span of each rotor. The CVC wake model directly computes the rollup of the vortex sheet into tip vortices rather than relying on user input of rolled-up tip vortex properties. The blade loads in CHARM are calculated using a vortex lattice method. A trim solution is followed by a transient solution to capture the outwash in-ground effect in CHARM. The latter is needed to capture the unsteady "pulsing" nature of the flow field. The trim solution adjusts rotor collective to match a user-specified thrust, iterating between a periodic, average wake solution and blade solution. During the subsequent transient solution, the rotor collective is fixed at the trim value, and a time-marching solution is performed, updating the wake and blade solutions simultaneously at each time increment. CHARM uses specialized models to account for the diffusion and dissipation of vorticity as CHARM is an inviscid solver. Details of these models can be found in [5]. In the work performed here, no tuning of these models was performed to match test data – default settings suggested by prior work were used.

CHARM uses Eqn 4 to model vortex diffusion, where r_{c_0} is the initial core size of the element,ν is the kinematic viscosity, a_1 is the diffusion gain constant,and Γ_v is the vortex circulation strength.

$$r_c = \sqrt{{r_{c_0}}^2 + 5.0(\nu + a_1\Gamma_v)t} \tag{4}$$

In the CHARM analysis for this study, the full scale CH-47 rotor was characterized as a three-bladed rigid rotor with a tip speed of 706 ft/s. The blade planform had a 29.45 ft radius, 20% cutout, 1.76 ft chord, and 12 degrees of linear washout from the hub to tip with a NACA 0012 airfoil profile along the full span of the blade. The rotor blades were modeled with a single row of 80 equal-spaced vortex lattice quadrilaterals. The induced velocities were calculated and stored at 24 azimuth locations while running the case for 200 revolutions for the trim solution followed by 400 time-marching revolutions during the transient solution. A high number of revolutions is required to properly capture the long-time, pulsing nature of the wake solution in ground effect, as the wake extends down to the ground and expands into the outwash region to the far field. CHARM allows the user to select the number of vortex filaments and the number of vortex elements (BCVE's) along each filament to use in the CVC wake model. In the present study, the wake was

modeled with 7.5 turns of full-span wake followed by 60 turns of single tip filament wake with up to 20 vortex filaments released from the full span of each rotor blade.

V. Results and Discussion

A. Single Rotor OGE

Before evaluating the actuator line model's ability to predict outwash, a preliminary study is completed for a single rotor operating in an OGE condition. This initial case serves to establish a baseline for rotor wake prediction and to assess the capabilities and limitations of the actuator line model. This subsection begins with a high-level, qualitative comparison of wake predictions from blade-resolved and actuator line models, followed by a quantitative evaluation of both load and wake predictions. One key objective of implementing the actuator line model in this study is to achieve wake predictions with reasonable accuracy while significantly reducing computational costs compared to the blade-resolved approach. Therefore, discussions on modeling fidelity will be accompanied by considerations of the computational costs associated with each numerical model examined.

For the OGE case presented in this section, both the blade-resolved and actuator line-based OVERFLOW simulations completed 20 rotor revolutions before extracting rotor wake predictions. Before comparing rotor-induced velocity profiles, rotor wake structures computed using both CFD-based modeling approaches were compared. To understand the differences in the predicted wake structure, an isometric visualization of the computed rotor wake is provided in Fig. 6. In Figure 6, an isosurfaces of Q-criterion contoured by the coefficient of pressure are plotted for both the (a) blade-resolved and (b) actuator line models. Provided the current thrust deviations between the two models, wake predictions between Fig. 6 (a) and (b) can be not directly correlated one-to-one. Despite this limitation the current high-level qualitative visualizations still demonstrate both notable similarities and several fundamental differences between the two numerical approaches.

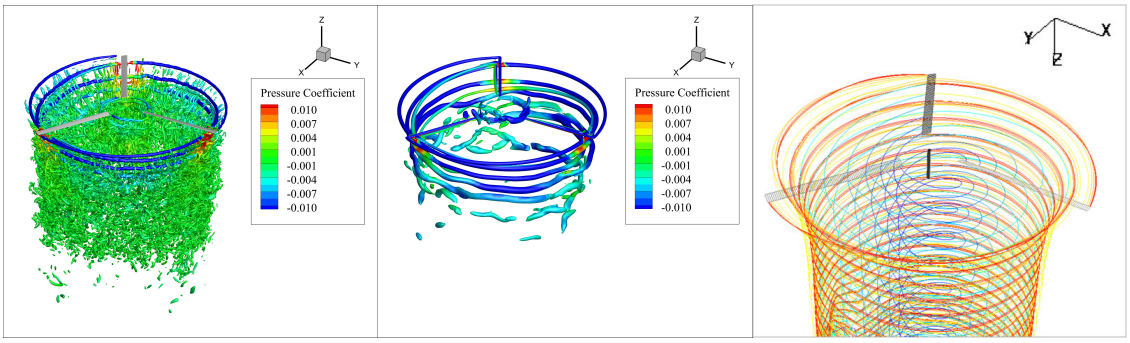

(a) Blade-Resolved (b) Actuator Line (c) CHARM

Fig. 6 Isometric view of blade-resolved and actuator line rotor wake predictions. Graphic shows iso-surface of (a,b) q-criterion contoured by coefficient of pressure, and (c) filament.

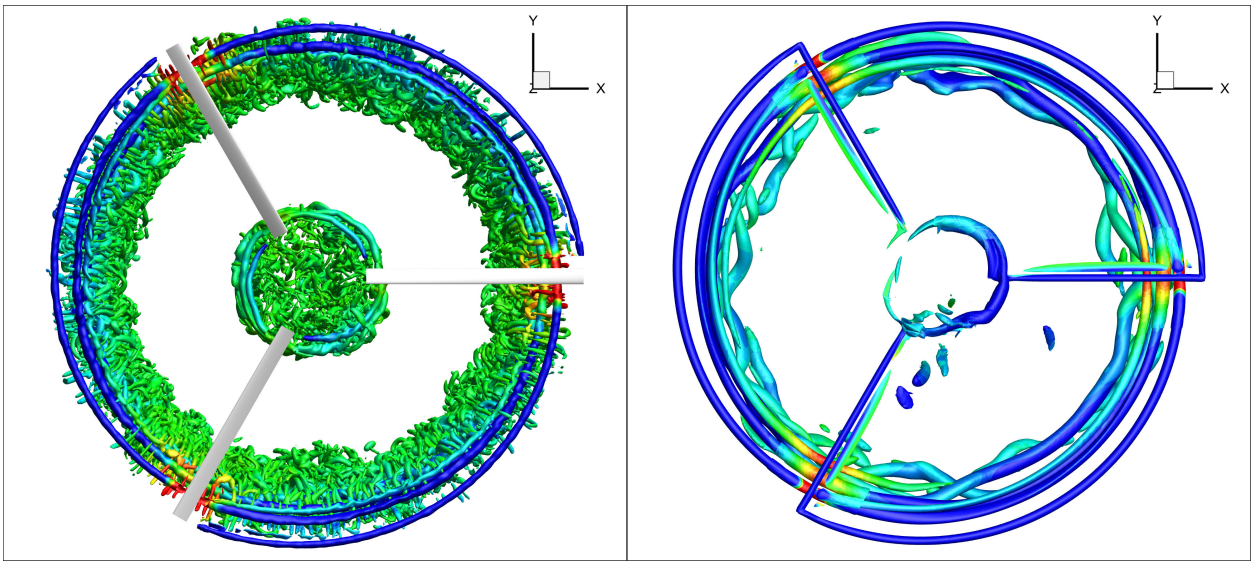

(a) Blade-Resolved (b) Actuator Line

Fig. 7 XY-plane view of blade-resolved and actuator line rotor wake predictions. Graphic shows iso-surface of q-criterion contoured by coefficient of pressure. Contour levels are consistent with Fig. 6.

At a high level, this qualitative observation of rotor tip vortices demonstrates a reasonable consistency between the two modeling approaches. Figures 6 and 7 illustrate how vortices follow a reasonably similar trajectory for approximately one to two revolutions. Furthermore, results shown in Fig. 7 provides evidence that Blade Vortex Interaction (BVI) consistently occurs near the 90% radial station for both models. These initial observations are consistent with predictions based on fundamental aerodynamic circulation theory. If the actuator line and blade-resolved models represent a comparable spanwise loading gradient, circulation theory would suggest that the generated rotor tip vortices should have similar strengths between the two models. For accurate predictions of the induced velocity profile, considering that rotor tip vortices largely influence rotor-induced velocities, the observed similarity between the two numerical models suggests the potential feasibility of using a simplified actuator line model for reasonably accurate predictions of the rotor wake at a reduced computational cost.

However, further observation of Fig. 6 clearly indicates fundamental differences between the two CFD modeling approaches; the differences are illustrated in the ZY-plane visualization presented in Fig. 8. Figure 8 shows a ZY-plane extract contoured by gray scaled vorticity magnitude contours. To assist in appreciating the correlation between the two dimensional plane extract and the full three-dimensional wake structure, isosurfaces of Q-criterion are superimposed on the visual while being blanked out in the negative Y-axis.

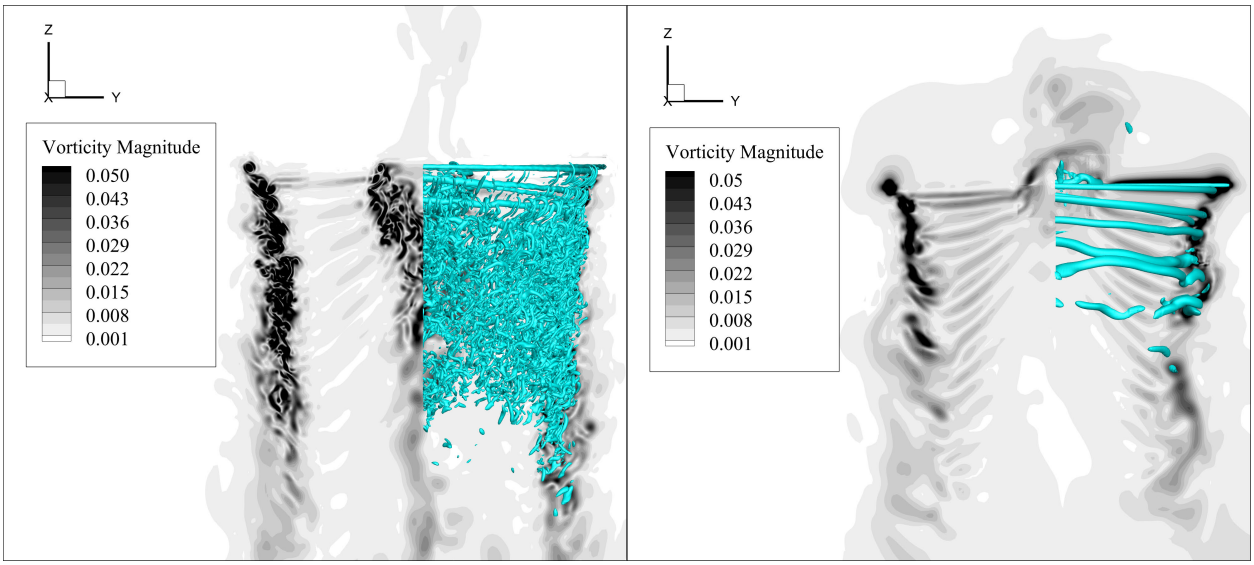

(a) Blade-Resolved (b) Actuator Line

Fig. 8 ZY-plane view of actuator line rotor wake predictions. Graphic shows iso-surface of q-criterion with a ZY-plane extract of vorticity magnitude.

Closer observation of the two rotor wakes, as shown in Fig. 8, highlights the notably different wake ages at which the rotor tip vortices appear to break down. Figure 8 demonstrates that blade-resolved simulated rotor tip vortices appear to break down relatively quickly after forming. However, rotor tip vortices computed using the actuator line model instead appear to remain coherent for several rotor revolutions, and up to one rotor radii below the rotor. To help appreciate why this fundamental difference in wake breakdown exists, a close-up of the blade-resolved rotor tip vortex formation is provided in Fig. 9. Figure 9 (a) presents six plane slices distributed along the rotor's tip chord contoured by vorticity magnitude. Isosurfaces of Q-criterion are shown with labels pointing to the preliminary vortices leading to the final rotor tip vortex.

As has been observed in experimental measurements presented by Duraisamy et. al [46], when flat tip faces are used for a given rotor blade, two vortices are first formed along the rotor's tip face. As the flow transverses from the lower to upper surfaces of the rotor, initial flow separation generates two separate vortices, labeled in Fig. 9 as *Bottom Vortex* and *Top Vortex*. These vortices first form near the leading edge of the rotor's tip face. As the two vortices further develop, the *Top Vortex* transverses further inboard while the *Bottom Vortex* slowly convects to the suction side of the blade. Eventually, as shown in Fig. 9, the *Bottom Vortex* and *Top Vortex* merge to form a single tip vortex, labeled as *Tip Vortex* in Fig. 9 (b). When implementing the actuator line modeling approach, the tip vortex formation is greatly simplified by comparison. This reduced-order modeling approach has no flow separation or interactions with wall boundaries. Rather, in this simplified rotor model, a single point exists at the rotor's tip, about which the tip vortex forms, greatly simplifying the process of the vortex's generation.

As with any reduced-order model, it is important to highlight that there are several factors that could be driving the observed differences in wake prediction. One potential factor driving differences in wake breakdown could feasibly be the selected source term distribution function. Relatively small deviations in the applied source term distribution function can greatly influence the wake predictions of an actuator line model. For example, in previous work completed by Churchfield et. al an alternative actuator line modeling approach was investigated [34]. In this alternative approach, a chordwise distribution was accounted for in the source model. In their work, this alternative source term modeling approach provided a notable variation in the predicted wake structure. As such, it is reasonable to presume that further iteration of the current lifting line modeling approach may be required to increase the fidelity of the current initial actuator line wake predictions.

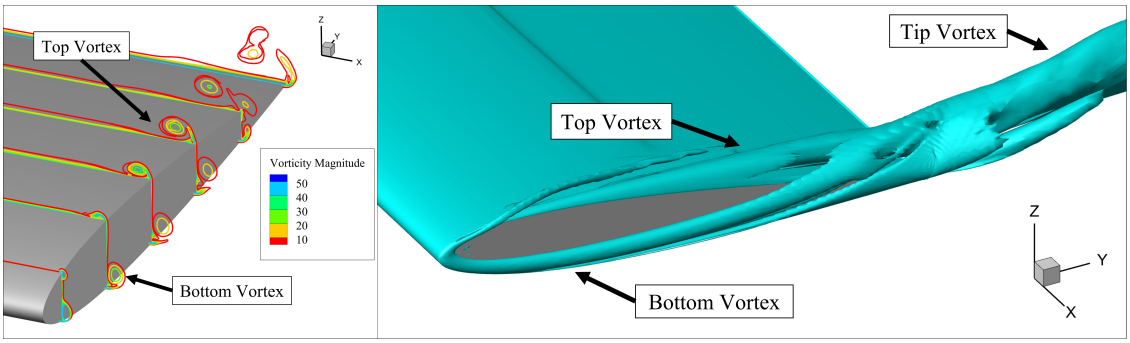

(a) (b)

Fig. 9 Visual of rotor tip vortex formation as computed through the blade-resolved representation.

Ranging from source term distribution modeling to mesh refinement, there ultimately exists a broad range of potential contributing factors that could be driving deviations between the blade-resolved and actuator line wake predictions. However, preceding any of these factors is the spanwise loading of the blade model. To identify similarities and differences in blade loading between the three modeling approaches, spanwise blade loadings were extracted from all three numerical methods investigated in this study. These blade loadings are presented in Fig. 10 and are shown as sectional normal force coefficients normalized by coefficient of thrust, $\frac{C_n}{C_T}$ versus radial location, $\frac{r}{R}$. For all three numerical approaches, blade loadings were extracted at one instance in time after 20 revs and plotted in Fig. 10.

Results show that both CHARM and actuator line modeling are consistently over predicting near the rotor tip, $\frac{r}{R} > 0.8$, and under predicting blade loading inboard, $0.3 < \frac{r}{R} < 0.8$, when compared to blade-resolved predictions. In the near tip region, maximum loading is over-predicted by 17%. Accurately capturing the influence of rotor tip vortices on spanwise loading when using line models has been a well-documented challenge in the rotorcraft community. In briefly summarizing this challenge, it is sufficient to highlight that the thrust loss due to a rotor's tip vortex is a complex, three-dimensional phenomenon, leading to a significant challenge in establishing a simplified model for capturing its effect on a one-dimensional line. In this study, a relatively simplistic tip loss model is used. This tip loss model simply establishes a linear taper to 0 in thrust after the blade's 98% radial station. Of further importance to highlight is the deviation in loading near the radial location of $\frac{r}{R} = 0.9$. Flow visualization presented in Fig. 7 indicates this spike in loading is likely due to BVI. As implemented in this study, both CHARM and actuator line modeling approaches appear to consistently over predict the influence of BVI on the blade loading coefficients. While this observed over-prediction of BVI appears to be drastic, further comparison of rotor wakes highlights the effect this difference plays on time-averaged wake predictions.

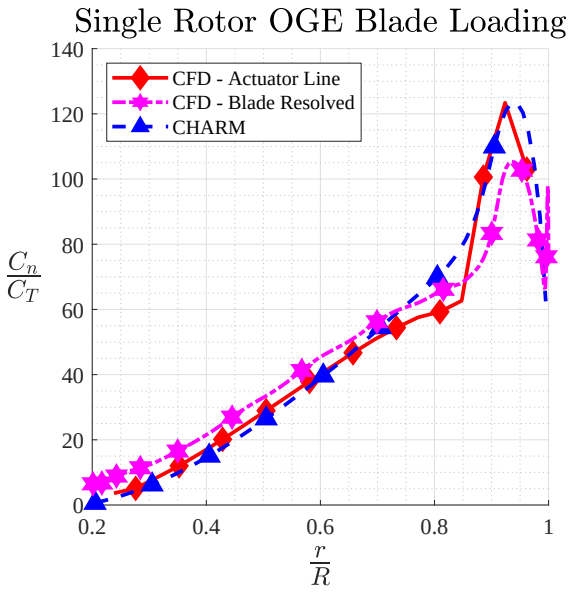

Fig. 10 Line plots for time averaged blade loadings.

With a greater appreciation of both the similarities and differences in both rotor wake structure and blade loading between the three numerical modeling approaches, rotor-induced velocity profiles were next extracted at four disk planes below the rotor. These disk planes consisted of 100 radial nodes and 37 evenly distributed azimuth nodes. Induced velocities were interpolated onto each node on the disk, after which the interpolated solutions were azimuthally averaged to produce a single velocity at each radial station. Averaged solutions were plotted in Fig. 11 for four distances beneath the rotor's hub, labeled as z/R where z is the vertical distance from the hub and R is the rotor radius. Solutions for induced velocity V are normalized by momentum theory induced velocity V_h which can be computed knowing rotor thrust coefficient C_T and tip speed V_{tip} ($V_h = V_{tip}\sqrt{C_T/2}$).

Despite differences in both wake structure, Fig. 6, and blade loading, Fig. 10, results for time averaged wake predictions show that a high degree of correlation is obtained between all three numerical modeling approaches and the experimental measurements. In particular, results presented in Fig. 11 demonstrate a near exact tracking is obtained between the actuator line and blade-resolved CFD simulations. Notably, actuator line predictions were obtained at a greatly reduced computational cost compared to the blade-resolved simulation. As shown in Table 1, CFD simulations completed using the actuator line model achieved a 80x reduction in core-hour computational cost compared to the blade-resolved simulation. In other words, at the same HPC core-hour cost, roughly 80 actuator line simulations could be completed for every 1 blade-resolved simulation. Despite running on nearly 1/5th the number of CPUs, the actuator line simulation required only 4 hours of compute time while the blade-resolved case required roughly 2.5 days. This computational cost reduced was achieved despite running using the same off-body solver settings between the two simulations.

Several key factors drive the computational cost reduction. First, by far the largest contributing factor driving the cost reduction is the prescribed time step. As previously mentioned, all blade-resolved CFD simulations in this study used time steps corresponding to 0.25° azimuth rotation per time step. Actuator line simulations were completed with time steps much larger, corresponding instead to 2° azimuth rotation per time step. As such, through simply accounting for time step variation, it would be assumed that roughly a 8x reduction in computational cost could be achieved. An additional factor driving this deviation in computational cost is the differences in total off-body cell count. As previously observed in Fig. 6, the blade-resolved simulation showed a higher degree of wake breakdown compared to the actuator line case. As such, despite using the same AMR input settings, the blade-resolved simulation required a total of roughly 150 million points for the off-body, while the actuator line case only resulted in a total of only 50 million points for the off-body solution. Furthermore, the blade-resolved simulation required 30 million points to represent the rotor while the actuator line case only required 6 million points in this study. This difference in total cell count further drives the observed differences in total required CPU count to run these simulations. A plethora of merited arguments exist for reducing cost of both the blade-resolved and actuator line simulation.

Clearly, further investigation is warranted regarding various CFD-based cost reduction measures, particularly for

Table 1 Comparison of approximate computational cost between actuator line, blade-resolved, and CHARM numerical approaches for single CH-47D rotor OGE.

Value	Blade-Resolved (20 revs)	Actuator Line (20 revs)	CHARM (600 revs)
CPUs	1,200	224	8
Hours	60	4	4
Core Hours	72,000	896	32

outwash applications [22]. Despite these caveats the observed computational cost reductions and retained modeling fidelity are still noteworthy. Reported cost reductions are reasonably consistent with cost savings observed in the literature [47], and additionally highlight the potential advantages of using the actuator line model to provide an increased number of rotor wake predictions while still retaining the modeling fidelity of the blade-resolved solution.

In discussing computational cost savings, the CFD solutions do not exist in isolation and are not the only numerical approach for rotor wake predictions. The rotorcraft community commonly relies on low cost, mid-fidelity comprehensive analysis tools, such as CHARM, to rapidly obtain a broad range of solutions within the rotorcraft design space. To help reduce computational cost, these comprehensive analysis tools commonly leverage vortex panel, and CVC wake models to predict the rotor's wake. While the tuning process for building these wake models can require a significant degree of user expertise and ground truth data, once tuned the models are capable of providing meaningful predictions for a broad range of applications at a greatly reduced computational cost compared to CFD simulation [5]. Results presented in Fig. 11 and Table 1 further help highlight this statement. Once the proper implementation of the CHARM wake model has been identified, wake predictions can be obtained on what is essentially laptop level computational hardware at time of writing. This is particularly true at wake depths of $\frac{z}{R} = -3.2$, at which point wake predictions become indistinguishable from the CFD solutions and experimental measurements. In the current case, results of this comparison are perhaps intuitive to the reader as the present demonstration case in this section is for a relatively simplistic setup. As modeling complexity increases in the proceeding sections, computational savings are further investigated to identify whether the identified cost savings hold.

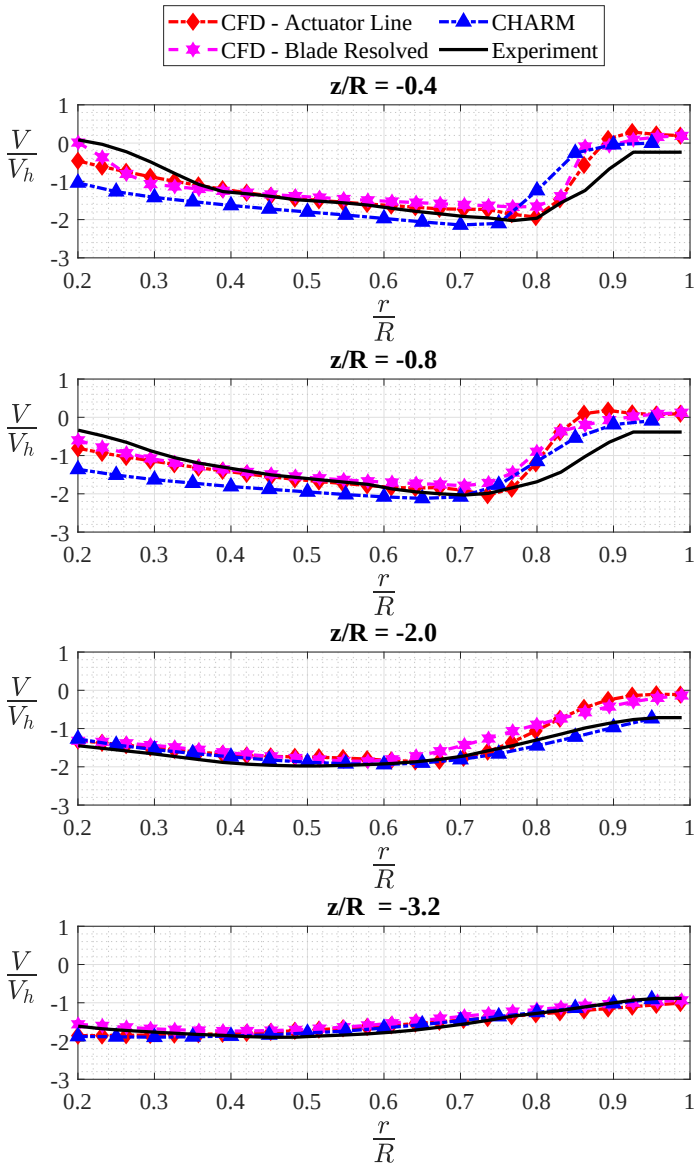

Fig. 11 Averaged induced velocity profiles.

B. Single Rotor IGE

With a baseline achieved for each numerical approach's ability to predict rotor wakes, outwash predictions are now demonstrated. The aim of this subsection is to assess the relative predictive capability of each numerical method to predict outwash generated by a single rotor. Single-rotor configurations are largely not representative of typical AAM rotor configurations. However, in evaluating single rotor outwash, this study aims to further establish a baseline for each numerical approach. Once again, numerical approaches are evaluated based on both the accuracy of their solutions and their computational costs. In presenting results for this subsection, a preliminary qualitative wake comparison is first briefly introduced. A quantitative comparison of numerical predictions for blade loading, maximum averaged outwash, outwash boundary layers, and PAXman model predictions are then presented.

Both actuator line and blade-resolved CFD simulations completed 30 rotor revolutions to develop an initial outwash wake. Figure 12 visualizes the developed outwash for both CFD approaches, showing iso-surfaces of the q-criterion contoured by the pressure coefficient, and CHARM filaments in ground effect. The contour levels and iso-values are consistent between graphics (a) and (b). Consistent with observations in the previously shown in Fig. 6, while the rotor

tip vortices follow a similar trajectory, the actuator line wake predictions are notably more diffused compared to those from the blade-resolved simulations. The wake predictions obtained from the blade-resolved simulation (Fig. 12 (a)) indicate that tip vortex breakdown occurs close to half a rotor radius beneath the rotor's hub. In contrast, the actuator line results show that the tip vortices remain coherent for a longer duration. These results are observed despite largely consistent off-body numerical approaches used in both simulations. Several factors may contribute to the differences in the predicted wake structure, including variations in the selected source term kernel and mesh refinement. Although addressing these discrepancies is beyond the scope of the current study, further investigation to minimize the differences in predicted wake structures is recommended. However, regarding the application of time-averaged outwash predictions, it remains uncertain whether small deviations in unsteady wake structures have a meaningful impact on rotor wake predictions. Therefore, in the context of this study, the rotor wake predictions are considered acceptable for further analysis.

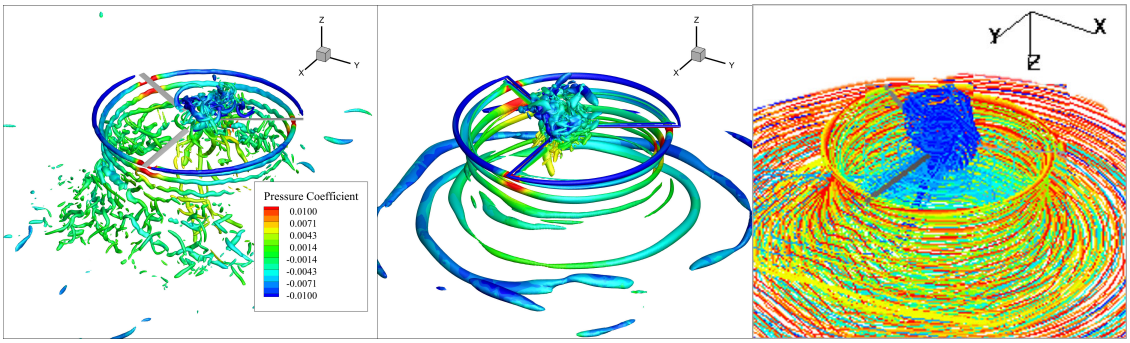

(a) Blade-Resolved (b) Actuator Line (c) CHARM

Fig. 12 Isometric view of blade-resolved and actuator line rotor outwash predictions. Graphic shows iso-surface of (a, b) q-criterion contoured by coefficient of pressure, and (c) filament.

After an initial startup wake was developed, blade loading predictions from each numerical simulation were saved and time averaged such that a blade loading comparison could be completed. Spanwise blade loadings were saved at 2° intervals and averaged over the course of 10 rotor revolutions. Resulting time averaged loadings are presented in Fig. 13. Results presented in Fig. 13 convey a comparable message to that of Fig. 10. Results show that both CHARM and actuator line modeling are consistently over predicting near the rotor tip, $\frac{r}{R} > 0.8$, and under predicting blade loading inboard, $0.3 < \frac{r}{R} < 0.8$, when compared to blade-resolved predictions, with maximum percent error of 12%. Despite persisting deviations compared to blade-resolved simulation, results presented in Fig. 13 demonstrate that both the CHARM and actuator line predictions of a single rotor remain largely consistent in both OGE and IGE operating conditions.

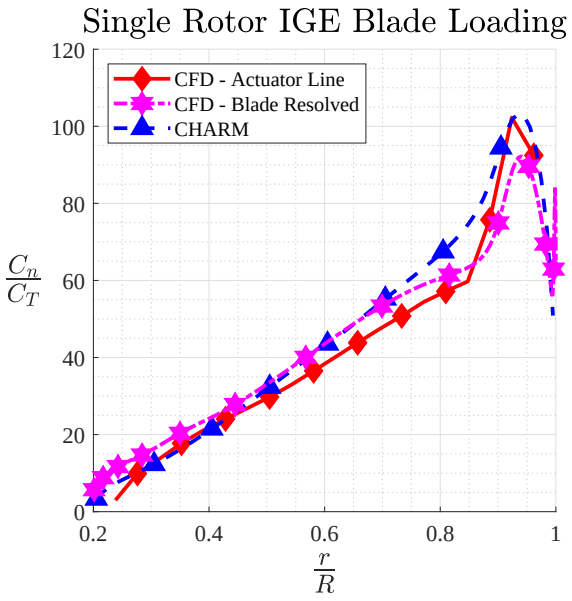

Fig. 13 Line plots for time averaged blade loadings.

With relative blade loading established between the three numerical modeling approaches, rotor outwash predictions can now be evaluated. In this discussion, maximum velocities of the time averaged flow field are first compared. For both CFD simulations, the velocity flow field was time averaged over the course of 10 rotor revolutions while presented CHARM solutions are time averaged over 300 revolutions. Solutions are then extracted azimuthily about the rotor's hub and are further averaged to find outwash boundary layer profiles at various radial distance from the rotor's hub. The maximum velocities of the boundary layers as a function of radial distance are presented in Fig. 14 for all three numerical approaches. In Figure 14, velocities are normalized by momentum theory induced velocity and radial distance from the rotor's hub is normalized by rotor diameter. One of the primary objectives of this study is to establish the loss in modeling fidelity when using an actuator line model as opposed to full-order, blade-resolved simulation for outwash predictions. Results presented in Fig. 14 appear to demonstrate that, at least for time averaged flow fields, a comparable level of modeling fidelity is achieved for outwash predictions when using both blade-resolved and actuator line based modeling approaches. Both modeling approaches appear to closely track one another between $0.5 \leq r/D \leq 2$. While the blade-resolved solutions do briefly diverge from actuator line predictions between $1.5 \leq r/D \leq 2$, these solutions quickly realign before $r/D = 2$. Additional, both CFD solutions provide a similar degree of fidelity compared to the available experimental measurements, with predictions closely matching experimental averages and staying well within the reported bounds of uncertainty. Yet, results presented in Fig. 14 only demonstrate predicted maximum time averaged outwash, results which can potentially be misleading in understanding accuracy of the time averaged outwash solution. For instance, results presented in Fig. 14 appear to indicate that CHARM is over predicting the desired outwash profile. While this may be correct in terms of maximum time averaged outwash, a closer comparison of outwash boundary layer profiles tells a more complete story.

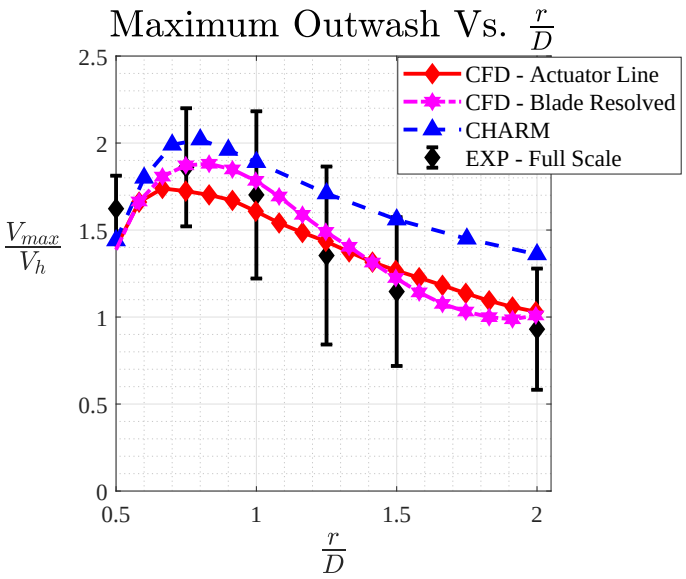

Fig. 14 Maximum, time averaged outwash predictions as achieved through all three numerical approaches investigated in this study.

Figure 15 presents outwash boundary layer predictions using each numerical approach at six radial distances from the rotor's hub, ranging from $0.5 \leq r/D \leq 2$. Results are plotted up to a height of 12 feet or $z/D = 0.2$. In reviewing the outwash boundary layer results presented in Fig. 15, a number of key conclusions can be drawn. First, CHARM is producing a close tracking of the experimental measurements at all six reported radial distances. Results shown in Fig. 14 appeared to indicate an over prediction of outwash from CHARM. However, closer observation of Fig. 15 rather indicates this over prediction is largely isolated to the near wall region of the outwash profile ($z/D < 0.03$ *or* < 2 *ft*). For heights higher than $z/D = 0.03$, CHARM provides meaningful outwash predictions over a broad range of heights and distances from the rotor's hub. The second key conclusion from Fig. 15 is the apparent under prediction of outwash when using the actuator line model as implemented in this study. For heights above $z/D = 0.1$, line model predictions consistently under predict outwash profiles compared to both the experiment and the blade-resolved simulation. Several factors could be driving this reduction in numerical fidelity. However, conclusions previously drawn from Fig. 12 may provide one viable explanation for the observed fidelity loss. As previously discussed, Fig. 12 demonstrates that actuator line produced wakes, as modeled in this study, contained significantly less turbulence compared to the blade-resolved results. This decreased turbulence appears to limit mixing between layers in the flow field, resulting in outwash which in some instances is higher near the wall and lower away from the wall compared to the blade-resolved solutions. This explanation remains only a hypothesis currently, but highlights the need for identifying an improved actuator line modeling approach capable of more accurately capturing wake unsteadiness present in blade-resolved simulations.

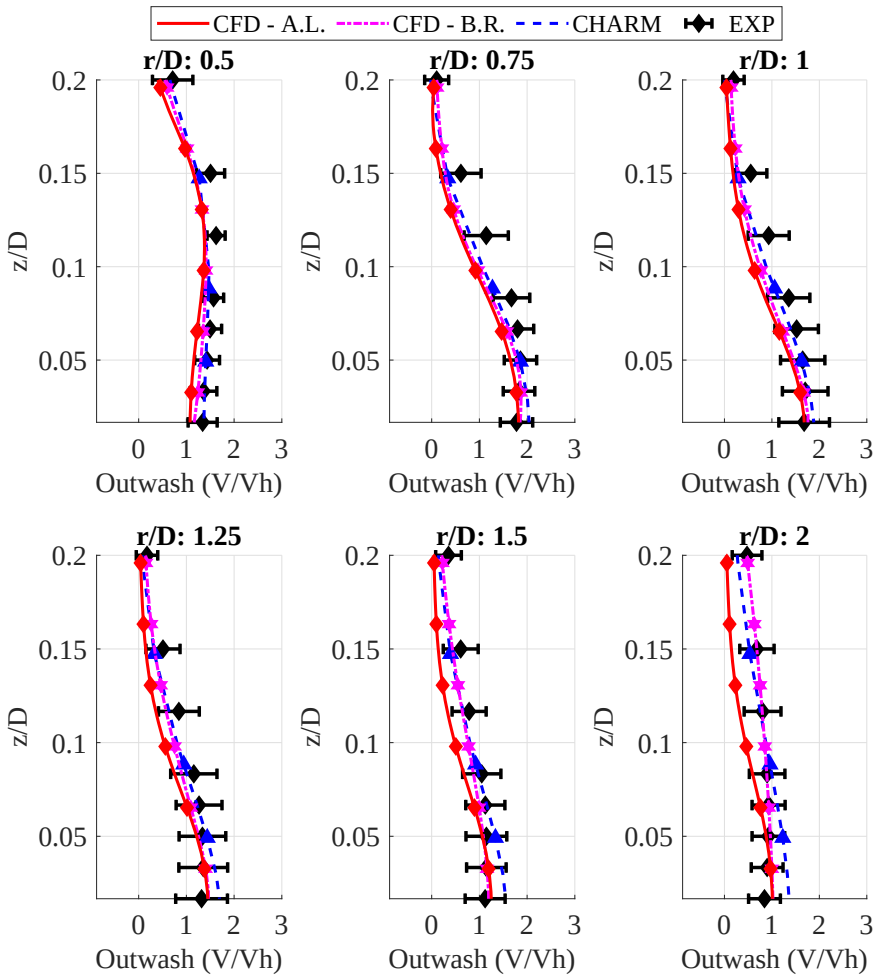

Fig. 15 Outwash boundary layer profiles as computed through all three numerical approaches investigated in this study.

Despite these limitations, for heights below z/D =0.1, actuator line model predictions are shown to closely match the experimental measurements. This subregion of the boundary layer is arguably the most relevant to capture for practical applications. Below z/D =0.1 is where the landing pad ground crew and ground support equipment are found and is reasonably the area of highest importance for accurately predicting outwash. To better gauge outwash prediction accuracy in terms of ground operations, outwash profiles are integrated using the PAXman model. Results presented in Fig. 16 clearly demonstrate that both the actuator line and blade-resolved solutions consistently provide a close tracking of the experimental measurements, with a near exact prediction achieved for $r/D = 2$. Results additionally demonstrate the CHARM model is able to provide meaningful predictions across all radial locations looked at in this study.

In this subsection, a wide range of comparisons were drawn between actuator line and blade-resolved simulations for a single rotor hovering IGE. Presented comparisons included qualitative wake predictions, blading loadings, maximum outwash profiles, outwash boundary layer profiles, and PAXman model predictions. Throughout each comparison, results obtained when using the actuator line model were consistently shown to provide a reasonable level of fidelity compared to the blade-resolved results. This level of fidelity was achieved while greatly reducing the total computational cost required to obtain the outwash prediction. As shown in Table 2, total core-hour cost of the actuator line model was 50x lower than that of the blade-resolved simulations. As has been iterated in the previous subsection, there are a list of contributing factors driving this reduction in computational cost. Yes, in terms of single-rotor time-averaged outwash predictions, a significant computational savings can be achieved with an acceptable drop in fidelity when implementing the actuator line model as opposed to that of a blade-resolved simulation.

Table 2 Comparison of approximate computational cost between blade-resolved, actuator line, and CHARM numerical approaches for single CH-47D rotor IGE.

Value	Blade-Resolved (40 revs)	Actuator Line (40 revs)	CHARM (600 revs)
CPUs	1,440	336	8
Hours	140	12	5
Core Hours	201,600	4,032	40

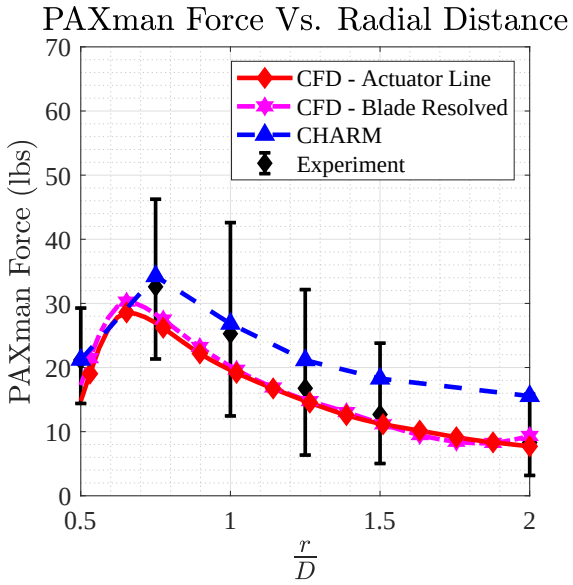

Fig. 16 PAXman model predictions as obtained using actuator line, blade-resolved, and CHARM models compared to experimental measurements.

C. Tandem Rotor IGE

In the previous two subsections, results were presented for both single rotor OGE and IGE cases. Despite vast differences in the numerical approaches, all three computational models have thus far been demonstrated to provide a reasonable degree of fidelity when compared to experimental measurements. While the prior demonstration cases discussed in this paper are essential for establishing a foundational understanding of modeling capabilities, they may not accurately represent actual AAM-based downwash and outwash scenarios. In simplifying the computational domain to a single rotor, this study was able to establish the fundamental modeling capabilities and limitations for wake structure, blade loading, and downwash/outwash predictions. However, when considering single rotor configurations, time-averaged prediction metrics become azimuth independent, thus greatly reducing complexity of the domain of interest. As such, in this subsection the complexity is increased by investigating a tandem rotor configuration. In this configuration, outwash predictions become more challenging to predict as the outwash becomes highly directional. As previously mentioned in the introduction of this paper, multi-rotor configurations notoriously generate directional, increased velocity outwash jets at the intersection of the two rotors' wakes. These jets are further non-symmetric about the vehicle y = 0 lateral plane owing to the counter rotation of the two rotors; note that axis corresponds as 17. To help illustrate the complexity of tandem rotor outwash, flow visualizations for both blade-resolved and actuator line predicted fields are shown in Fig. 17. While difficult to dissern from Fig. 17, flow visualization shows an increased amount of turbulence present in the tandem rotor configuration as opposed to the single rotor configuration. This increased production of turbulence appears to be most prevalent along the rotor's x = 0 plane, a region which contains the previously mentioned starboard and port outwash jets. The objective of this subsection is to identify the fidelity of

time averaged, numerical predictions in these highly turbulent starboard and port outwash jets. However, before time averaged outwash predictions can be compared, deviations in rotor blade loadings must be established.

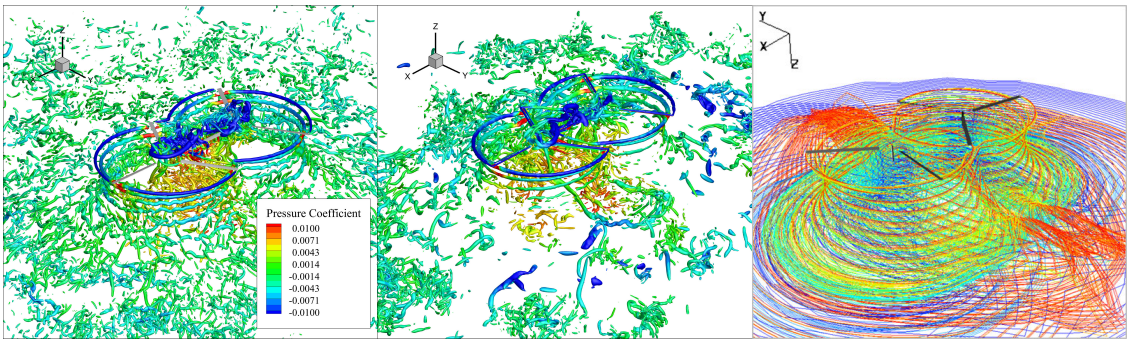

(a) Blade-Resolved (b) Actuator Line (c) CHARM

Fig. 17 Isometric view of blade-resolved and actuator line rotor outwash predictions. Graphic shows iso-surface of (a, b) q-criterion contoured by coefficient of pressure, and (c) filament.

The tandem rotor configuration introduces a significant source of increased modeling complexity when prediction blade loads. In the current configuration, significant rotor overlapping is prescribed, with rotor hubs spaced roughly 1.3 radii apart. To obtain accurate predictions for rotor outwash in the x = 0 plane, reasonably accurate rotor loading predictions are needed this overlap region. Yet, as demonstrated in Fig. 17, there clearly exists a significant degree of unsteadiness in the flow field within this overlap region. As such, in order for consistent outwash predictions to be achieved, the actuator line model must be capable of providing comparable load predictions as blade-resolved within the overlap region. To compare blade loadings between CHARM, actuator line, and blade-resolved simulations, solutions for blade loading were saved at 2° azimuth rotation over the 10 rotor revolutions. Solutions were then the averaged across all 10 revolutions. Contour plots for all three numerical approaches are provided in Fig. 18 as contours of $\frac{C_n}{C_T}$ for the front rotor. Despite the increased aerodynamic complexity present, results shown in Fig. 18 demonstrate a reasonably close comparison is still achieved between all three numerical approaches. Between azimuth positions of 90° and 270°, contours appear to show all three numerical approaches provide blade loading predictions with comparable deviations as was identified in the single rotor cases. Further evidence of this low level of discrepancy can be found in Fig. 19. Figure 19 shows line plots of blade loading for all three numerical approaches at four azimuth locations corresponding to Fig. 18. For azimuth positions, 90°, 180°, and 270°, a close comparison is achieved between all three numerical approaches.

Within the rotor overlap region, found between azimuth positions of 315° and 45°, a reasonable degree of loading discrepancy can additionally be found. Given the significant differences in modeling between the three numerical approaches, it is perhaps intuitive that loading deviations exist within the highly turbulent overlap region. As indicated in Fig. 19 azimuth of 0°, each model is providing a distinct blade loading prediction within this region. Results presented in Fig. 18 show CHARM predicting a relatively 'smooth' overlap region in comparison to that of the blade-resolved simulation. Deviations between CHARM and blade-resolved in this subregion can largely be explained by differences in wake modeling. The blade-resolved simulation is capable of reasonably accurately capturing the turbulence present within the overlap region, something CHARM is not feasibly able to model. In contrast, actuator line predictions do appear to provide a closer tracking of the blade-resolved loading solution within the overlap region. Blade loading peak present near the rotor tip and an azimuth of 10° appears to be captured reasonably well, and overall both models provide a reasonably similar loading prediction.

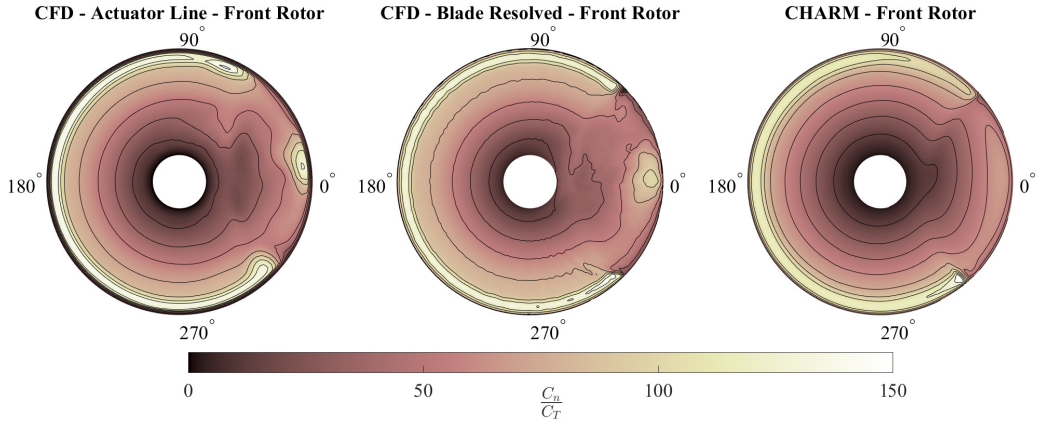

Fig. 18 Contour plots for time averaged blade loadings for the forward counter clockwise rotating front rotor. Graphic includes actuator line (left), blade-resolved (center), and CHARM (right) predictions.

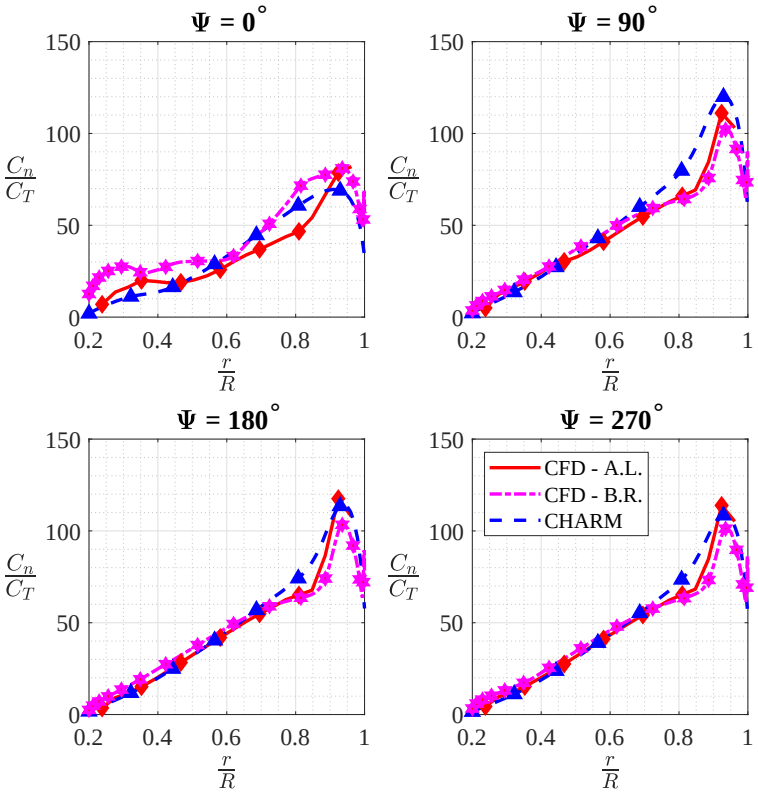

Fig. 19 Line plots for time averaged blade loadings at four azimuth positions of the rotor. Azimuth positions are consistent with labels in Fig. 18.

With deviations in blade loading established, outwash predictions in both the port and starboard sides can now be reviewed. Before extracting the outwash profiles, both CFD simulations were conducted for 30 revolutions to ensure that an initial outwash wake was fully developed. The velocity flow field was time-averaged over 10 rotor revolutions, while the presented CHARM solutions were averaged over 300 revolutions. The results were extracted along the x = 0 plane in both the starboard and port directions to obtain time-averaged boundary layer profiles. Figure 20 shows the maximum velocities of the boundary layers as a function of distance from the centerline for all three numerical

approaches. In Figure 20, the velocities are normalized by the velocity predicted by momentum theory, and the distance from the centerline is normalized by rotor diameter. A diagram show radial axis (r) and radial velocity (V_r) in the starboard and port directions is provide Fig. 3.

Figure 20 (a) demonstrates actuator line port side outwash predictions are achieved at a degree of fidelity close to blade-resolved simulations. Time averaged maximum outwash velocities exhibit a near exact tracking between the two modeling approaches for the full radial distance range tracked in this study. Consistent with previous observations identified in Fig. 15, port side outwash boundary layer predictions shown in Fig. 21, are largely consistent with blade-resolved below z/D =0.1. Further integration of the outwash through the PAXman model demonstrate a reasonably close prediction is achieved between the CFD modeling approaches. The PAXman prediction results can be found in Fig. 23 (a). However, a similarly high degree of tracking on the starboard side is not observed in Fig. 20 (b). While for $\frac{r}{D} > 1.25$ actuator line predictions are achieved within the experimental uncertainty, starboard actuator line outwash predictions are notably lower than the blade-resolved counter part. The observed outwash reduction is additionally found throughout the starboard outwash boundary layer, as shown in Fig. 22. Integration of the starboard boundary layers further shows the actuator line model to provide a notably lower force prediction compared to blade-resolved predictions. The PAXman prediction results can be found in Fig. 23 (b).

While further work is required to identify the driving factor for the starboard reduced outwash velocity predictions, two possible factors were identified in this study. The first factor driving this observed difference could be the reduced turbulence present in the actuator line simulation compared to the blade-resolved simulation. While difficult to discern from Fig. 17, closer observation of the starboard outwash indicates a strong outwash 'jet' is formed in this subregion of the flow field. The effect of this jet can be seen in Fig. 20, as maximum values of the experimental data on the starboard side are shown to be higher than that of the port side. Both CHARM and blade-resolved simulations show higher outwash velocities on the starboard side as opposed to the port side. However, actuator line results appear to be nearly identical between both port and starboard sides. It is possible the reduced level of turbulence present in the actuator line simulation is driving the lack of variation between port and starboard sides. The second factor driving this observation could also be the lack of adding drag source terms in the current actuator line implementation. As implemented in the current study, only lifting forces are includes in the source term model. When considering the counter rotation of the tandem rotors, it remains feasible that adding drag source terms may increase modeling fidelity in the starboard direction. Despite the observed modeling differences, the actuator line model is still providing a reasonably high level of fidelity in outwash predictions. Boundary layer predictions, particularly near an $\frac{r}{D} = 2$, are shown to consistently fall within the bounds of uncertainty for the experiment. Further integration of the boundary layer shows actuator line predictions remain within the uncertainty of the experiment for $\frac{r}{D} > 1$.

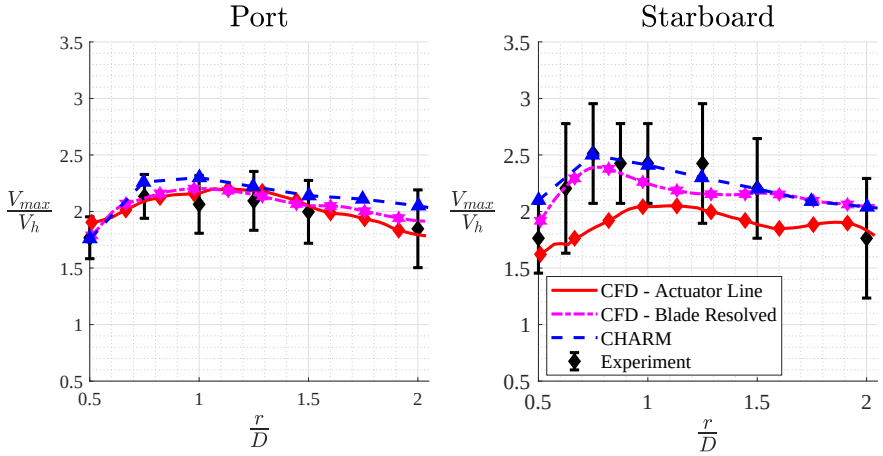

Fig. 20 Maximum, time averaged outwash predictions as achieved through all three numerical approaches investigated. Port side predictions are shown in the left graphic while starboard predictions are shown in the right graphic.

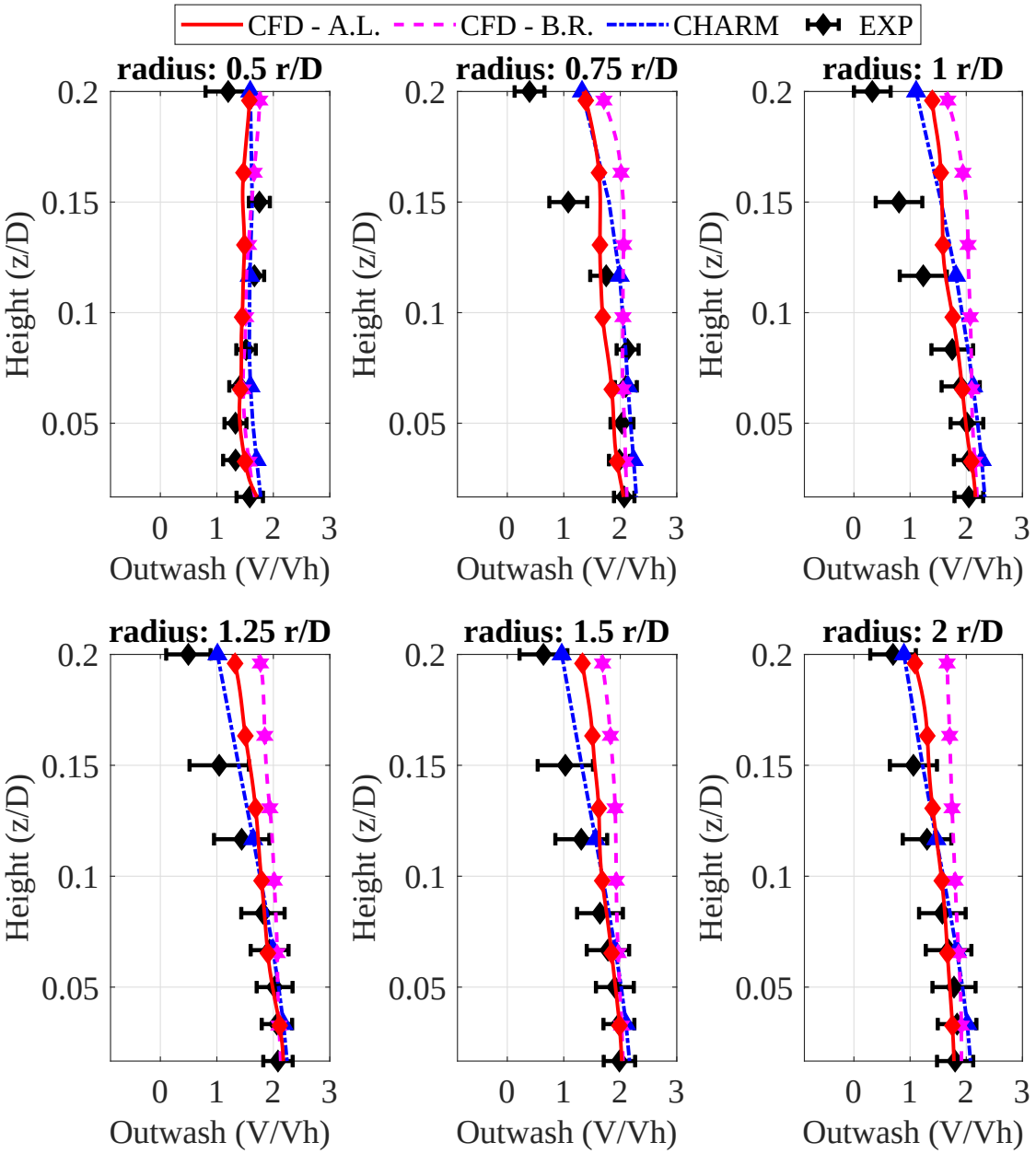

Fig. 21 Port outwash boundary layer profiles as computed through all three numerical approaches investigated in this study.

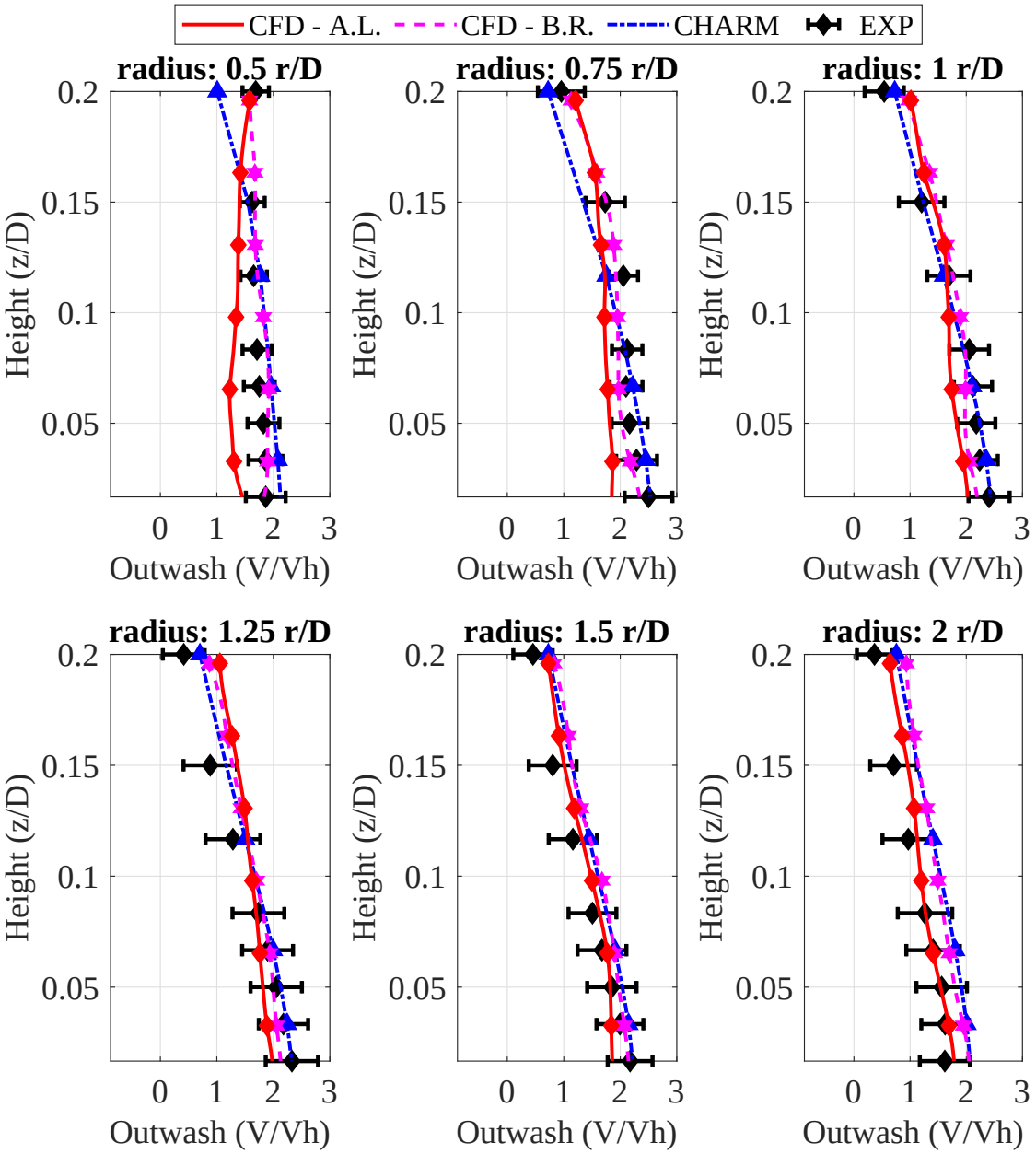

Fig. 22 Starboard outwash boundary layer profiles as computed through all three numerical approaches investigated in this study.

Table 3 Comparison of approximate computational cost between actuator line, blade-resolved, and CHARM numerical approaches for tandem configuration IGE.

Value	Blade-Resolved (40 revs)	Actuator Line (40 revs)	CHARM (600 revs)
CPUs	1,440	336	8
Hours	240	30	15
Core Hours	345,600	10,080	120

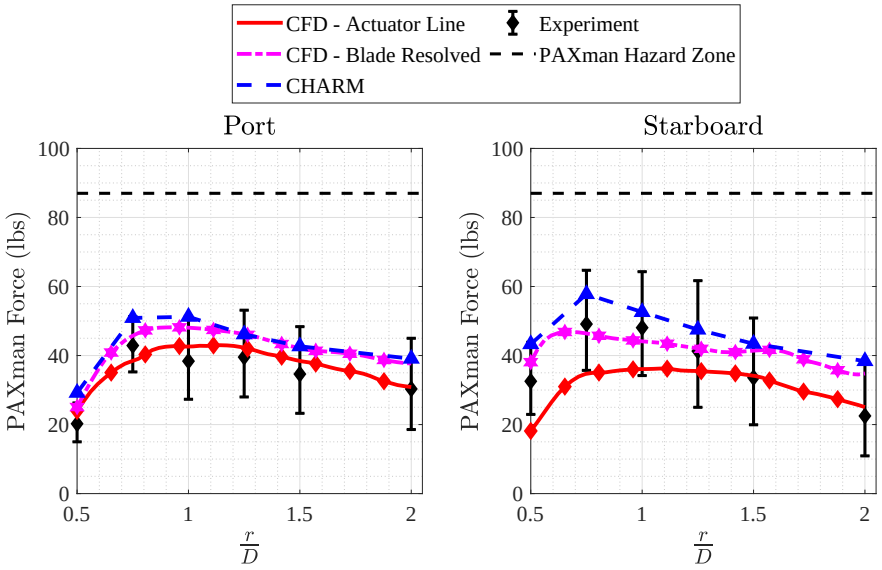

Fig. 23 PAXman model predictions as obtained using actuator line, blade-resolved, and CHARM models compared to experimental measurements.

VI. Conclusions

This study's objective was to provide the reader with an appreciation of the advantages and limitations of deploying a CFD-based actuator line modeling approach for reduced computational cost, reasonable-fidelity time averaged outwash predictions. In pursuit of this objective, the study aimed to identify both the modeling fidelity loss of actuator line compared to blade-resolved simulation, and the role actuator line models reasonably fill within the modern rotorcraft design toolchain. The authors aimed to achieve these objectives through the demonstration of three, progressively more complex demonstration cases, namely: single rotor OGE, single rotor IGE, and tandem rotor IGE. The metrics explored in this study included blade loading, time-averaged maximum outwash velocities, and integrated outwash predictions using the PAXman model. Results demonstrated that for the metrics analyzed in this study, actuator line modeling achieves a reasonably low loss of fidelity compared to blade-resolved simulation.

Moreover, when considering CPU core-hour cost metrics, actuator line predictions were consistently achieved using well over an order of magnitude reduction in computational expense compared to the blade-resolved simulations. For the single rotor IGE comparison, actuator line simulations were 80 times cheaper than their blade-resolved counterparts. Similarly, for single-rotor OGE the actuator line simulations were also 50 times cheaper. Additionally, as illustrated in Table 3, the tandem rotor outwash predictions from this study achieved time-averaged outwash predictions at a core-hour cost that was 34 times lower than that of blade-resolved simulations. One key objective of this study was to evaluate both modeling fidelity and cost of actuator line outwash predictions compared to those of blade-resolved simulation. Results clearly indicate, at least for time-averaged outwash predictions, that actuator line simulation is an efficient and reasonably accurate approach for predicting both single and multi-rotor outwash.

Despite this observed reduction in computational cost for the actuator line model, actuator line simulations still required hundreds of CPUs and several hours of compute time. Comparatively, results shown in Tables 1, 2, and 3 demonstrate CHARM predictions were achieved using far fewer resources than that of the CFD models. It is noted that for CHARM-like models to be effectively leveraged for outwash predictions, a preliminary tuning of the wake model must be completed. Once this preliminary tuning is completed, results shown in this study consistently demonstrated the reasonably high degree of fidelity with which CHARM was able to predict both single and multi-rotor outwash. One notable limitation of using the CHARM model for outwash predictions is the challenge of identifying relevant experimental data to tune the wake model. This issue is particularly acute for AAM vehicles, which have limited publicly available experimental datasets. In the absence of such data, design teams inevitably rely more heavily on CFD simulations. Provided the current limitations of actuator line multi-rotor outwash predictions, it is clear that blade-resolved CFD simulations should still be primarily used for obtaining initial sampling of new rotor configurations and operating conditions.

With a preliminary validation for numerical outwash predictions established, future work of this study will focus on exploring ways for improving actuator line multi-rotor outwash predictions. Both new source term distribution functions and adding drag source terms will be explored. Additionally, future work will focus on further reducing computational cost associated with using the actuator line model. This future study will include both further mesh refinement studies and GPU acceleration.

Future work will also expand the actuator line model currently implemented in the OVERFLOW code. The OVERFLOW-based actuator line model implemented in this paper is a preliminary NASA internal model, with a primary intended application for rotorcraft outwash predictions. As such, future work for this study includes expanding the actuator line validation effort to encompass a broader range of applications relevant to the rotorcraft community.

Acknowledgments

The authors express their gratitude to Ethan Romander, Gloria Yamauchi, Wayne Johnson, Chris Silva, and Sesi Kottapalli for their valuable feedback in reviewing this paper. Authors would like to thank Carlos Pereyra for creating post-processing script for RCOTOOLS to be used for CHARM Contour results. Thank you to Dan Wachspress for his excellent feedback and recommendations. Additionally, the authors would like to acknowledge William Warmbrodt, Thomas Norman, and Noah Schiller for supporting this study.

References

[1] Schane, W., "Effects of Downwash Upon Man," USAARU Report No. 68-3, 1967. URL `https://apps.dtic.mil/sti/pdfs/AD0662208.pdf`.

[2] George, M., Perlmutter, A., and Butler, L., "Downwash Impingement Design Criteria for VTOL Aircraft," TRECOM Technical Report 64-48, 1964. URL `https://apps.dtic.mil/sti/pdfs/AD0608185.pdf`.

[3] Preston, J. R., Troutman, S., Keen, E., Silva, M., Whitman, N., Calvert, M., Cardamone, M., Moulton, M., and Ferguson, S. W., "Rotorwash operational footprint modeling," RDMR-AF-14-02, 2014. URL `https://apps.dtic.mil/sti/pdfs/ADA607614.pdf`.

[4] Sabbagh, L., "Flying Blind in Iraq: U.S. Helicopters Navigate Real Desert Storms," *Popular Mechanics*, 2009. URL `https://www.popularmechanics.com/military/a5540/4199189`.

[5] Wachspress, D., Whitehouse, G., Yu, K., Gilmore, P., Dorsett, M., and McClure, K., "A High Fidelity Brownout Model For Real-time Flight Simulations and Trainers," *Proceedings of the 65th Annual American Helicopter Society Forum.*, Grapevine, Texas, 2009.

[6] Rovere, F., Barakos, G., and Steijl, R., "CFD Analysis of a Micro-Rotor in Ground Effect," *45th European Rotorcraft Forum.*, Warsaw, Poland, 2019.

[7] Merabet, R., and Laurendeau, E., "Numerical simulations of a rotor in confined areas including the presence of wind," *Aerospace Science and Technology*, Vol. 126, 2022, p. 107657. https://doi.org/https://doi.org/10.1016/j.ast.2022.107657, URL https://www.sciencedirect.com/science/article/pii/S1270963822003315.

[8] Silva, M., and Riser, R., "CH-47D Tandem Rotor Outwash Survey," *Proceedings of the 67th Annual American Helicopter Society Forum.*, Virginia Beach, Virginia, 2011.

[9] Ramasamy, M., and Yamauchi, G. K., "Using Model-Scale Tandem-Rotor Measurements in Ground Effect to Understand Full-Scale CH-47D Outwash," *Journal of the American Helicopter Society*, Vol. 62, No. 1, 2017, pp. 1–14. https://doi.org/doi:10.4050/JAHS.62.012004, URL https://www.ingentaconnect.com/content/ahs/jahs/2017/00000062/00000001/art00004.

[10] Conley, S., Peters, N., Aires, J., Wagner, L., Kallstrom, K., Withrow-Maser, S., Wright, S., Radotich, M., Chianello, C., Rivera, G. O., et al., "VTOL Analysis for Emergency Response Applications (VAERA)-Identifying Technology Gaps for Wildfire Relief Rotorcraft Missions," *6th Decennial VFS Aeromechanics Specialists' Conference*, VFS, Santa Clara, California, 2024.

[11] Aires, J., Withrow-Maser, S., and Peters, N., "Utilizing Advanced Air Mobility Rotorcraft Tools for Wildfire Applications," *Proceedings of the 80th Annual Forum and Technology Display*, VFS, Montreal, Quebec, Canada, 2024.

[12] Silva, C., and Solis, E., "Aircraft Design Implications for Urban Air Mobility Vehicles Performing Public Good Missions," *Proceedings of the 80th Annual Forum and Technology Display*, VFS, Montreal, Quebec, Canada, 2024.

[13] Johnson, M., "Advanced Capabilities for Emergency Response Operations (ACERO)," *NASA/JAXA Meeting on Disaster Response Aeronautics Research*, 2022.

[14] Zimbelman, T., Dailey, L., Oriach, D., Flom, N., and Metcalfe, M., "Advanced air mobility missions for public good," , No. NASA/CR–20230012505, 2023.

[15] "NASA Urban Air Mobility (UAM) Reference Models," , 2024. URL https://sacd.larc.nasa.gov/uam-refs/.

[16] Wernicke, R., "Prediction of Tilt Rotor Outwash," *19th Annual Aerospace Sciences Meeting*, AIAA, Fort Worth, Texas, 1981. 10.2514/6.1981-13.

[17] Leishman, J. G., *Principles of Helicopter Aerodynamics*, Cambridge University Press, Cambridge, England, 2006, Chap. 14.

[18] Ferguson, S., "Rotorwash Analysis Handbook Volume I - Development and Analysis," FAA, DOT/FAA/RD-93/21, June 1994.

[19] Tan, J. F., Sun, Y. M., and Barakos, G. N., "Vortex approach for downwash and outwash of tandem rotors in ground effect," *Journal of Aircraft*, Vol. 55, No. 6, 2018. https://doi.org/10.2514/1.C034740.

[20] Moushegian, A. M., and Smith, M. J., "Physics and Accuracy of Dual-Solver Simulations of Rotors in Ground Effect," *Journal of the American Helicopter Society*, Vol. 68, No. 1, 2023, pp. 1–16. https://doi.org/doi:10.4050/JAHS.68.012010, URL https://www.ingentaconnect.com/content/ahs/jahs/2023/00000068/00000001/art00010.

[21] Goericke, J., Habana, Z., Batther, J., and Muia, M., "Downwash/Outwash Investigation in Support of eVTOL Landing Operations," *6th Decennial Aeromechanics Specialists' Conference.*, Santa Clara, California, 2024.

[22] Caprace, D.-G., Ventura Diaz, P., and Yoon, S., "Simulation of the Rotorwash Induced by a Quadrotor Urban Air Taxi in Ground Effect," *Proceedings of the 79th Annual Forum and Technology Display*, VFS, West Palm Beach, Florida, 2023.

[23] Chaderjian, N., "A Quantitative Approach for the Accurate CFD Simulation of Hover in Turbulent Flow," *Journal of the American Helicopter Society*, Vol. 68, 2023. https://doi.org/10.4050/JAHS.68.042009.

[24] Ventura Diaz, P., Johnson, W., Ahmad, J., and Yoon, S., "The Side-by-Side Urban Air Taxi Concept," *Proceedings of the AIAA Aviation Forum*, AIAA, Dallas, Texas, 2019. 10.2514/6.2019-2828.

[25] Ventura Diaz, P., and Yoon, S., "High-Fidelity Simulations of a Quadrotor Vehicle for Urban Air Mobility," *Proceedings of the AIAA SciTech Forum*, AIAA, San Diego, California, 2022. 10.2514/6.2022-0152.

[26] Garcia Perez, D., Ventura Diaz, P., and Yoon, S., "A Comparison of Rotor Disk Modeling and Blade-Resolved CFD Simulations for NASA's Tiltwing Air Taxi," *79th VFS annual forum*, VFS, West Palm Beach, Florida, 2023.

[27] Narducci, R. P., Jain, R., Abras, J., and Hariharan, N. S., "HVAB Rotor Hover Computational Prediction: A Comparative Study Using OVERFLOW and HPCMP CREATE™-AV Helios," *AIAA Scitech 2021 Forum*, VIRTUAL EVENT, 2021. https://doi.org/10.2514/6.2021-0617, URL https://arc.aiaa.org/doi/abs/10.2514/6.2021-0617.

[28] Klimchenko, V., Min, B.-Y., and Wake, B., "Model and Full-Scale Rotor Hover Performance Analysis using HELIOS/OVERFLOW," *AIAA SCITECH 2023 Forum*, National Harbor, Maryland, 2023. URL https://arc.aiaa.org/doi/abs/10.2514/6.2023-1188, 10.2514/6.2023-1188.

[29] Chan, W., Gomez, R., Rogers, S., and Buning, P., "Best Practices in Overset Grid Generation," *32nd AIAA Fluid Dynamics Conference*, St. Louis, Missouri, 2002. 10.2514/6.2002-3191.

[30] Merabet, R., and Laurendeau, E., "Parametric study on the velocity sampling techniques for the actuator line method in 2D," *Proceedings of the AIAA SciTech Forum*, AIAA, San Diego, California, 2019. 10.2514/6.2019-1797.

[31] Jude, D., Hosseinverdi, S., Sitaraman, J., Péron, S., and Boisard, R., "Actuator Line and Immersed Boundary Methods for Rotorcraft CFD," *80th VFS annual forum*, VFS, Montreal, Quebec, Canada, 2024.

[32] Chiew, J. J., and Aftosmis, M. J., "Integral Velocity Sampling for Unsteady Rotor Models on Cartesian Meshes," *Proceedings of the AIAA Aviation Forum*, AIAA, VIRTUAL EVENT, 2021. https://doi.org/10.2514/6.2021-2624.

[33] Forsythe, J. R., Lynch, E., Polsky, S., and Spalart, P., "Coupled Flight Simulator and CFD Calculations of Ship Airwake using Kestrel," *Proceedings of the AIAA SciTech Forum*, AIAA, Kissimmee, Florida, 2015. https://doi.org/10.2514/6.2015-0556.

[34] Churchfield, M. J., Schreck, S. J., Martinez, L. A., Meneveau, C., and Spalart, P. R., "An advanced actuator line method for wind energy applications and beyond," *35th Wind Energy Symposium*, AIAA, 2017, p. 1998. 10.2514/6.2017-1998.

[35] Flemming, R., "An Experimental Evaluation of Advanced Rotorcraft Airfoils in the NASA Ames Eleven-Foot Transonic Wind Tunnel," 1984. NASA/CR–166587.

[36] Kallstrom, K., and Shirazi, D., "Airfoil Table Generation and Validation for the VR-12 and SSC-A09 Airfoils and Quadrotor Performance Prediction," *6th Decennial VFS Aeromechanics Specialists' Conference*, VFS, Santa Clara, California, 2024.

[37] Weist, L., Schatzman, N., and Shirazi, D., "Best Practices for Predicting Acoustics of a Single Rotor Using the NASA RVLT Conceptual Design Toolchain," *6th Decennial VFS Aeromechanics Specialists' Conference*, VFS, Santa Clara, California, 2024.

[38] Stich, G.-D., Fernandes, L. S., Duensing, J. C., Housman, J. A., Kenway, G. K., and Kiris, C. C., *The 11th International Conference on Computational Fluid Dynamics*, ICCFD11, Maui, Hawaii, 2022.

[39] Wadcock, A. J., "Rotor Outwash," Unpublished Presentation Made to U.S. Army, 2005.

[40] Peters, N. J., and Pereyra, C., "RotorGen: A Simplified Structured Grid Generation Program for High-Fidelity Rotor CFD Simulation," *Presented at the AIAA 2024 Overset Grid Symposium*, Dayton, Ohio, 2024.

[41] Bliss, D., Teske, M., and Quackenbush, T., "A New Methodology for Free Wake Analysis Using Curved Vortex Elements," *NASA CR 3958*, CDI Report No. 84-6, December, 1987.

[42] Quackenbush, T., Bliss, D., Wachspress, D., Boschitsch, A., and Chua, K., "Computation of Rotor Aerodynamic Loading in Forward Flight using a Full-Span Free Wake Analysis," *NASA CR 177611*, CDI Report No. 90-05, October, 1990.

[43] Quackenbush, T., Lam, C.-M., and Wachspress, D., "Computational Analysis of High Resolution Unsteady Airloads for Rotor Aeroacoustics," *NASA CR 194894*, CDI Report No. 93-12, May, 1994.

[44] Boschitsch, A., Curbishley, T., Quackenbush, T., , and Teske, M., "A Fast Panel Method for Potential Flows About Complex Geometries," *AIAA-96-0024, AIAA 34th Aerospace Sciences Meeting & Exhibit*, Reno, NV, January 1996.

[45] Boschitsch, A., Usab, W. J., and Epstein, R., "Fast Lifting Panel Method," *AIAA-99-3376, AIAA 14th Computational Fluid Dynamics Conference*, Norfolk, VA, June 1999.

[46] Duraisamy, K., Ramasamy, M., Baeder, J. D., and Leishman, J. G., "High-Resolution Computational and Experimental Study of Rotary-Wing Tip Vortex Formation," *AIAA Journal*, Vol. 45, No. 11, 2007, pp. 2593–2602. https://doi.org/10.2514/1.26575.

[47] Wissink, A. M., Jude, D., Jayaraman, B., Roget, B., Lakshminarayan, V. K., Sitaraman, J., Bauer, A. C., Forsythe, J. R., and Trigg, R. D., "New capabilities in CREATE-AV helios version 11," *Proceedings of the AIAA SciTech Forum*, AIAA, Virtual Meeting, 2021, p. 0235. 10.2514/6.2021-0235.